Journal of Geoscience and Environment Protection, 2026, 14(11), 69-97
https://www.scirp.org/journal/gep
ISSN Online: 2327-4344
ISSN Print: 2327-4336

The Effects of High Groundwater Table on the Stability of Civil Engineering Infrastructure in Mombasa Island, Mombasa County, Kenya

Charles Ngala Kithome*, Edwin W. Dindi, Charles Maina Gichaba

Department of Earth and Climate Sciences, Faculty of Science and Technology, University of Nairobi, Nairobi, Kenya
Email: *charliekithome@gmail.com

How to cite this paper: Kithome, C. N., Dindi, E. W., & Gichaba, C. M. (2026). The Effects of High Groundwater Table on the Stability of Civil Engineering Infrastructure in Mombasa Island, Mombasa County, Kenya. *Journal of Geoscience and Environment Protection, 14,* 69-97.
https://doi.org/10.4236/gep.2026.1411004

Received: October 5, 2026
Accepted: November 16, 2026
Published: November 19, 2026

Copyright © 2026 by author(s) and Scientific Research Publishing Inc.
This work is licensed under the Creative Commons Attribution International License (CC BY 4.0).
http://creativecommons.org/licenses/by/4.0/
Open Access

Abstract

Mombasa Island, Kenya, is a raised Pleistocene coral-reef platform of weathered, karstic limestone and loose coastal soils that is undergoing rapid multi-storey development, yet routine site investigations report bearing pressures for dry conditions only. This study evaluated the effects of a high groundwater table on infrastructure stability on Mombasa Island and adjoining Nyali by integrating trial-pit, laboratory, dynamic cone, vertical electrical sounding, cone penetration and borehole standard penetration test (SPT) data, secondary electrical resistivity tomography (ERT) and multichannel analysis of surface waves (MASW) records, and Water Resources Authority groundwater records from nine screened datasets. The main water table beneath the raised platform lies about 15 - 20 m deep, with provisional upper saturated zones from about 4 - 7 m, whereas on the Tudor Creek margin and in parts of Nyali it lies within about 3 - 10 m of the surface. The overburden is a silty gravel (c' = 5 - 10 kPa; φ' = 21˚ - 25˚) over weak coral limestone (UCS 10.6 - 12.3 MPa), and groundwater near Tudor Creek is aggressive to concrete (sulphate up to 2261 mg/L, class XA2; chloride of marine origin up to 15,181 mg/L, classes XS2/XS3). In soil-only sensitivity cases, raising the water table to the surface reduced the calculated allowable bearing pressure by 20% - 34%; it also reduced the bearing capacity of dense Tudor sands by about 45%, doubled their computed settlement and imposed uplift of 9.8 kPa per metre of submergence. Assumed scenarios of suction loss and coral softening, which were not measured, gave possible reductions of 62% - 74% and 10% - 40%, respectively. At two distressed sites in Nyali, cracked structures coincide with saturated, low-stiffness or cavernous ground. The groundwater table should therefore be treated as a design variable in Mombasa.

Keywords

Groundwater Table, Bearing Capacity, Coral Limestone, Foundation Stability, Karst, Seawater Intrusion, ERT, MASW, Mombasa Island

1. Introduction

Coastal cities are built on ground whose engineering behaviour depends strongly on water. The coastal water table is a dynamic surface that responds to rainfall recharge, tides, sea-level change, abstraction and leakage from urban water and sewer networks, and its position controls the effective stress, strength, stiffness and chemical environment of foundation soils and rocks (Bosserelle et al., 2022; Richardson et al., 2024). A rising water table reduces the effective overburden and the effective unit weight of soil beneath footings, imposes buoyant uplift on slabs and basements, softens porous rock and brings saline, sulphate-bearing water into contact with buried concrete. Over the last decade, these processes have been recognised as a distinct and growing coastal hazard, usually termed groundwater inundation or groundwater flooding, which can damage infrastructure long before visible marine flooding occurs (Rotzoll & Fletcher, 2013; Befus et al., 2020; Habel et al., 2020, 2024; Hill et al., 2023).

Mombasa, the second-largest city in Kenya and the gateway port of East Africa, is particularly exposed. Mombasa Island is a raised Pleistocene coral-reef platform bounded by the tidal Tudor Creek and by Port Reitz-Kilindini Harbour, and the adjoining Nyali area lies on the same reef limestone on the northern mainland (Caswell, 1953). The limestone is porous, fractured and locally karstic, and it is mantled by loose sands, silty gravels and fill. The county population reached 1,208,333 in 2019 (Kenya National Bureau of Statistics (KNBS), 2019), and low-rise traditional buildings are being replaced or extended by multi-storey apartments and hotels. Groundwater beneath the Tudor Creek margin is brackish to saline, with chloride up to 15,181 mg/L, and freshwater heads declined by 0.79 m between 2015 and 2025, while the local relative sea level rose by about 0.23 m (Kithome et al., 2026a; Kithome et al., 2026b). Regional sea-level rise along the Kenyan coast is about 3 mm per year, and the Mombasa urban core has been classified among the most vulnerable coastal segments in Kenya (Kagema & Muzirafuti, 2026). Nearly one-third of the county lies in the high or very high flood-risk classes (Omanga, 2024), and recent structural incidents, including the partial basement collapse and tilting of an 11-storey building under construction in April 2025, have raised public concern about the stability of buildings on the island (Oduor, 2025; Hussein, 2025).

Despite this, routine geotechnical investigations in Mombasa are commonly limited to one to three shallow trial pits, a dynamic cone penetrometer (DCP) test and a few laboratory tests, from which a single "safe bearing capacity" is recommended for dry conditions (Cransfield Material Testing Centre (CMTC), 2025).

The depth of the water table, its variability, and its effect on foundation stability are rarely quantified. Therefore, the objectives of this paper are i) to characterise the depth and variability of groundwater beneath Mombasa Island and adjoining Nyali from integrated geotechnical and geophysical data; ii) to determine the properties of the foundation materials and their sensitivity to saturation; iii) to assess the aggressiveness of the groundwater to buried concrete; and iv) to quantify the effects of a rising groundwater table on the bearing capacity, settlement and uplift of shallow foundations, using documented cases of structural distress as field evidence.

2. Study Area

2.1. Location, Climate, and Land Use

The study area comprises Mombasa Island (Mvita Sub-County), including the Tudor Creek margin, Mji wa Kale (Old Town) and Kizingo, and the adjoining Nyali Sub-County; the Dongo Kundu Special Economic Zone (SEZ), Mikindani and the runway ends of Moi International Airport on the mainland provide comparative data (Figure 1). The climate is hot and humid, with bimodal rainfall in the long rains (April-June) and short rains (October-December) and a mean annual rainfall of about 1040 mm (Omanga, 2024). The island's surface rises from the creeks to about 22 - 23 m above sea level (asl) along the Kizingo-Old Town axis, whereas the creek margins at Tudor and the lagoon margins at Dongo Kundu lie only a few metres above sea level. Drainage is short and radial towards the creeks and relies largely on an ageing drainage network, parts of which date from the Arab and colonial periods (The Star, 2023).

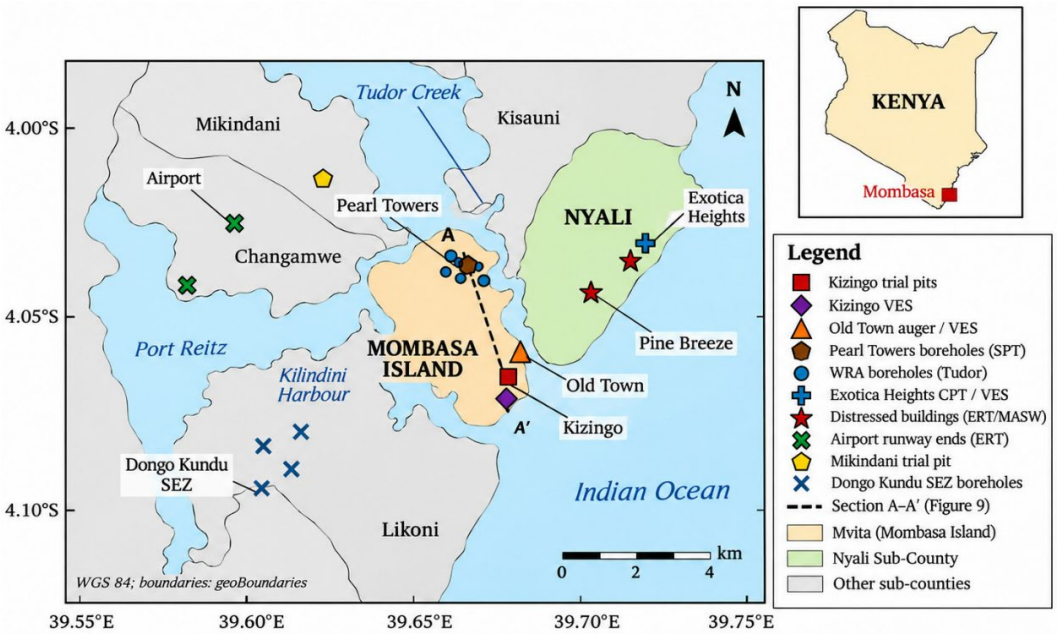


Figure 1. Study area map of the Mombasa-Nyali area showing the investigation sites, boreholes and geophysical surveys (WGS 84; ward and sub-county boundaries from geoBoundaries; site positions approximate).

2.2. Geology and Hydrogeology

The coastal plain is underlain by flat-lying Pleistocene coral reef limestone, lagoonal coral breccia, Shanzu calcarenite and Kilindini sands, which pass westwards into the Jurassic Kibiongoni beds and Changamwe-Kipevu shales and the Triassic-Permian Duruma sandstones (Caswell, 1953) (**Figure 2**). The reef limestone forms a highly permeable, fracture- and solution-dominated aquifer recharged rapidly by rainfall, leaking water mains and on-site sanitation (Oiro & Comte, 2019). The water table slopes gently towards the creeks, where groundwater discharges and tidal fluctuations propagate inland. In the Tudor aquifer, licensed abstraction increased from about 6000 to 14,000 m^3/day between 2015 and 2025 and mean freshwater head fell from 5.68 to 4.89 m asl, favouring seawater intrusion (Kithome et al., 2026a, 2026b).

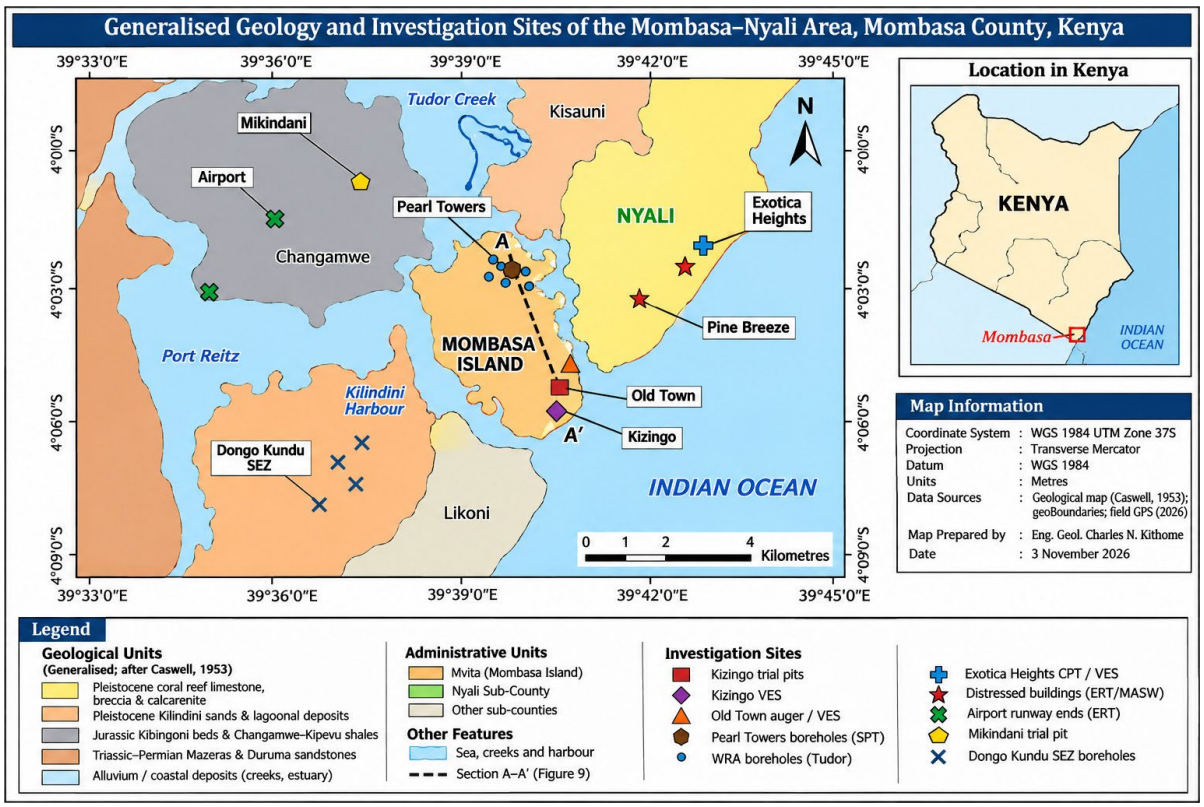


Figure 2. Generalised geology of Mombasa Island, Nyali and environs, with the investigation sites and the line of section A-A' (units generalised at ward level after Caswell, 1953; same base and site positions as **Figure 1**).

3. Materials and Methods

3.1. Data Sources

The study integrated nine datasets (**Table 1**). Primary data were obtained from site investigations in which the first author was the lead engineering geologist, and from the partner laboratory; secondary data comprised Water Resources Authority (WRA) groundwater records, a consultant's borehole and SPT report for Pearl Towers at Tudor (Paul Kimani & Company, 2018), a published factual

Table 1. Datasets used in the study.

Site	Data	Source
Kizingo, Nkrumah Road (22 m asl)	3 trial pits to 2.0 m; DCP; PSD, Atterberg, compaction, direct shear, point load	CMTC (2025)
Kizingo South	3 VES to AB/2 = 20 - 25 m	Field Data (2025/26)
Old Town, Baharini (23 m asl)	3 VES, 2 auger holes to 5 m, CU triaxial tests, soil chemistry, recorded groundwater observations	ARIDS (2022)
Tudor Creek Margin	16 WRA boreholes; heads 2015-2025; chemistry (n = 30, January-March 2025)	WRA Records; Kithome et al. (2026a)
Tudor, Pearl Towers (20 - 31 m asl)	2 boreholes to 30 m; SPT at 1 m intervals; index, density, CBR, shear box, chemistry	Paul Kimani & Company (2018)
Nyali, Exotica Heights	4 CPT, 4 VES	ARIDS (2026)
Nyali, Apartment Block	2 ERT (80 m), 7 MASW	Pro-Skill Engineers Hub (2025)
Nyali, Pine Breeze Resort	3 ERT (47.5 m), 2 MASW, crack survey	Pine Breeze Report (2025)
Moi International Airport; Dongo Kundu SEZ; Mikindani	2 ERT; 46 boreholes with SPT and CBR; 1 trial pit and laboratory tests	Pro-Skill Engineers Hub (2024); SECO (2021); CMTC (2026)

Note: CMTC = Cransfield Material Testing Centre; ARIDS = Aqua Rural Infrastructure Development Solutions; SECO = Southern Engineering Company.

report for the SEZ, and independent geophysical investigations of two distressed buildings in Nyali (an apartment block and Pine Breeze resort) and of the airport runway ends. All datasets were screened for traceability to dated field or laboratory records, internal consistency and physical plausibility. Pre-fieldwork synthetic models and untraceable schematic plots were excluded, as were the archived Old Town geophysical models (an ERT image, a three-dimensional resistivity mesh and a seismic refraction section) whose acquisition geometry could not be reconciled with the documented field programme, together with all quantities derived from them.

The groundwater chemistry dataset comprises 30 samples collected by the WRA between January and March 2025 from the 16 boreholes of the Tudor monitoring network, so some boreholes were sampled more than once; the sample allocation by borehole is reported in Kithome et al. (2026a). The descriptive statistics in Section 4.3 are computed over all 30 samples. Because repeat samples from the same borehole are not independent, the statistics are used only to assign exposure classes, not for spatial inference or significance testing. The groundwater heads (5.68 m asl in 2015 and 4.89 m asl in 2025) are network means of routine WRA water-level records. These records do not state whether each borehole was pumping, or the tidal phase and season at the time of measurement, so no correction for drawdown, tides or season could be applied. The heads are therefore used only to indicate the regional position of the water table and its decadal trend; because the 0.79 m decline is of the same order as possible tidal and seasonal variation, it is treated as indicative rather than exact.

3.2. Field and Geophysical Methods

Trial pits of 1.0 - 2.4 m depth were excavated mechanically and logged in accordance with BS 5930:2015+A1:2020, with groundwater observed during and after excavation. Boreholes at Pearl Towers were drilled to 30 m with standard penetration tests (63.5 kg hammer, 760 mm drop) at 1 m intervals, and water levels were recorded at the start and end of each drilling shift. The DCP (8 kg hammer, 575 mm drop) penetration index DN (mm/blow) was converted to California bearing ratio (CBR) and allowable pressure with the ASTM D6951 and Paige-Green and Du Plessis (2009) correlations:

$$\mathrm{CBR} = 292/\mathrm{DN}^{1.12};\ \ q_a = 3426.8\mathrm{DN}^{-1.0101}\,(\mathrm{kPa}) \tag{1}$$

Vertical electrical soundings used a Schlumberger array with AB/2 = 20 - 25 m, and the apparent resistivity $\rho_a = K\Delta V/I$ was inverted to layered models. Dar-Zarrouk parameters ($T = \Sigma h_i\rho_i$; $S = \Sigma h_i/\rho_i$) and Archie's law (Archie, 1942) were used to interpret conductive layers:

$$\rho_w = \rho_b n^m;\ \ EC_w = 10^4/\rho_w\,(\mu\mathrm{S/cm}) \tag{2}$$

with $a = 1$, $m = 2$ and porosity $n = 0.30$ - 0.40. Secondary two-dimensional ERT profiles (ABEM Terrameter LS; Lippmann 4-Point Light) used Wenner-Schlumberger or dipole arrays with 2 - 10 m electrode spacings and were inverted by smoothness-constrained least squares (Loke et al., 2013); the consultants' interpreted sections are reproduced, and the raw data were not reprocessed. MASW used a 24-channel Geometrics ES-3000 seismograph (Park et al., 1999); shear-wave velocities were converted to small-strain shear modulus $G_0 = \rho V_s^2$ and to indicative SPT N-values using $V_s = 97N^{0.314}$ (Imai & Tonouchi, 1982).

3.3. Laboratory Methods

Particle-size distribution, Atterberg limits (cone penetrometer), standard Proctor compaction and direct shear (specimens remoulded at 95% of maximum dry density) followed BS 1377; point-load tests on coral followed ASTM D5731, with UCS = 20.85 $I_{s(50)}$. Groundwater chemistry (sulphate, chloride, magnesium, pH) followed standard methods (American Public Health Association (APHA) et al., 2023), and aggressiveness was classified by BS EN 206 and BRE Special Digest 1 (British Standards Institution (BSI), 2021; Building Research Establishment (BRE), 2005). As specific gravity was not measured at Kizingo, $G_s = 2.70$ was assumed (values of 2.64 - 2.86 were measured at Pearl Towers) to derive void ratio, saturated and submerged unit weights:

$$e = G_s\rho_w/\rho_d - 1;\ \ \gamma_{sat} = \left[\left(G_s + e\right)/\left(1 + e\right)\right]\gamma_w;\ \ \gamma' = \gamma_{sat} - \gamma_w \tag{3}$$

3.4. Analytical Framework for Groundwater Effects

The ultimate bearing capacity of a square footing of width B at depth D_f was computed with Terzaghi's equation (Das & Sivakugan, 2019):

$$q_u = 1.3c'N_c + qN_q + 0.4\gamma_{eff}BN_\gamma \tag{4}$$

The effective surcharge q and unit weight γ_{eff} were modified for the water-table depth D_w:

$$D_w \le D_f:\ q = \gamma D_w + \gamma'\left(D_f - D_w\right);\ \gamma_{eff} = \gamma' \tag{5}$$

$$D_f < D_w \le D_f + B:\ q = \gamma D_f;\ \gamma_{eff} = \gamma' + \left[\left(D_w - D_f\right)/B\right]\left(\gamma - \gamma'\right) \tag{6}$$

$$D_w > D_f + B:\ q = \gamma D_f;\ \gamma_{eff} = \gamma \tag{7}$$

The allowable pressure was $q_a = q_u/3$, and the effect of the water table was expressed as the reduction ratio $R_w = q_u(D_w)/q_u(\text{dry})$. A water table at the surface ($D_w = 0$) also represents ponded surface water. The Terzaghi results were cross-checked with the general equation using Vesić factors and Meyerhof shape and Hansen depth factors. Settlement-controlled allowable pressure on the Tudor sands at Pearl Towers, where measured SPT data exist, was computed with the Meyerhof (1965) equation as modified by Bowles (1996) with $F_d = 1 + 0.33D_f/B \le 1.33$, and C_w:

$$q_a = 11.98\bar{N}\left[\left(3.28B+1\right)/\left(3.28B\right)\right]^2 F_d C_w;\ C_w = 0.5 + 0.5D_w/\left(D_f + B\right) \le 1 \tag{8}$$

and settlement with Burland and Burbidge (1985), $s = q'B^{0.7}(1.71/\bar{N}^{1.4})$, divided by C_w to represent a raised water table. Uplift on slabs and basements was $u = \gamma_w h_w$. The allowable pressure on coral rock followed Goodman (1989), $q_a = (\text{UCS}/5)(N_\varphi + 1)/15$ with $N_\varphi = \tan^2(45^\circ + \varphi/2)$ and $\varphi = 17^\circ$. All calculations were scripted in Python and validated against the laboratory's own dry-condition results. For the measured SPT at Pearl Towers, $\bar{N}$ was averaged from D_f to $D_f + B$ with refusals capped at $N = 50$. Two kinds of results are distinguished. Effects of the water table on effective stress, bearing capacity, settlement and uplift follow directly from the measured unit weights and strengths. Loss of suction-derived cohesion (c′ halved or removed on wetting) and saturation softening of the coral (softening coefficients $K_s = \text{UCS}_{sat}/\text{UCS}_{dry}$ of 0.6 - 0.9; Hawkins & McConnell, 1992; Vásárhelyi & Ván, 2006) were not measured and are treated as assumed sensitivity scenarios. The tools used and their alignment with the four objectives are summarised in **Table 2**.

4. Results

4.1. Subsurface Profile and Depth to Groundwater

At Kizingo (22 m asl), the trial pits showed 0.6 m of loose fill over red silty gravel with sand (GM) to 1.0 m and white, highly weathered, highly fractured coral from 1.0 m; no groundwater was encountered to 2.0 m (**Figure 3**). At Old Town (23 m asl), two auger holes encountered reddish-brown clayey silty sand to refusal at about 5 m (**Figure 4**). The deeper profile is interpreted in the project record as weathered, friable coral limestone, but it was not cored or sampled. The rock-quality (RQD) and SPT-equivalent values in the archived report were derived from a seismic model whose provenance could not be verified, so no RQD, rock strength or penetration values are assigned to Old Town in this paper. **Figure 4** therefore shows

only the auger, laboratory, VES and recorded groundwater evidence.

Table 2. Field, laboratory, and computational tools and their alignment with the objectives.

Objective	Field and Laboratory Tools	Analysis and Software	Output Used
1. Profile, groundwater, flood settings	Trial pits (backhoe), auger, boreholes with SPT, VES (Schlumberger), CPT, WRA boreholes, GPS; secondary ERT (ABEM Terrameter LS) and MASW (ES-3000)	BS 5930 logging; VES inversion; Dar-Zarrouk and Archie analysis; 2D models and sections (Python)	Depth to water and weak zones (Section 4.1)
2. Material properties	Sieves, cone penetrometer, Proctor, pycnometer, shear box, triaxial, point-load tester, CBR, DCP	USCS/AASHTO; Phase relationships; Mohr-Coulomb; Goodman rock bearing	Strength and unit weights (Section 4.2)
3. Aggressiveness	Groundwater and soil sampling; APHA and BS 1377-3 analyses	Statistics; BS EN 206, BRE SD1, BS 8500 classes	Concrete exposure classes (Section 4.3)
4. Stability effects	Outputs of 1 - 3; SPT, DCP, MASW	Equations (4) - (8); Burland-Burbidge; Uplift; Imai-Tonouchi (Python)	Reductions in q_a, settlement and uplift (Sections 4.4 - 4.6)

Source: This study.

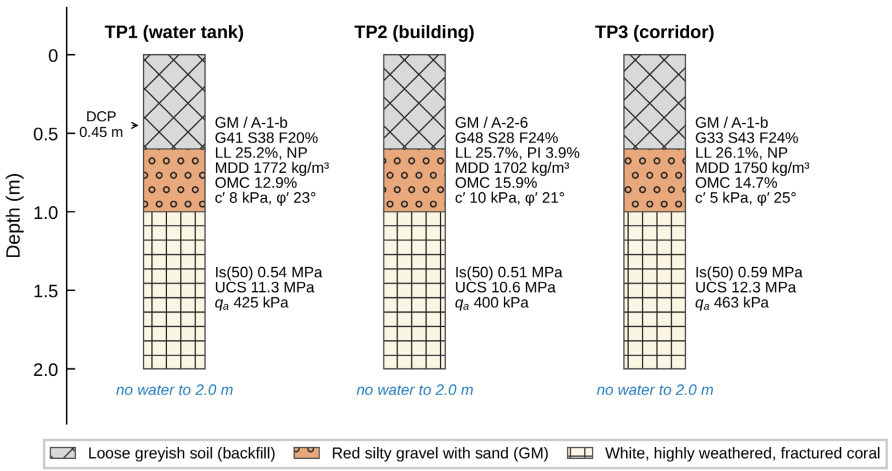


Figure 3. Trial-pit logs at Kizingo with index, strength and point-load data.

At Pearl Towers on the ground rising from Tudor Creek, two boreholes 62.77 m apart (ground 20 m and 31 m) were drilled to 30 m (**Figure 5**). BH01 penetrated 2 m of reddish-brown silty clay (N = 35) over dense coral fragments with sand to 9 m (N = 100, refusal) and medium-dense to dense silty sand to 30 m (N = 22 - 32); BH02 penetrated silty and gravelly sands (with N rising from 19 to 70) over 26 m of weak, weathered sandstone (UCS 0.31 - 0.43 MPa). The coral horizon of BH01 passes laterally into sand within 60 m. The sands are non-plastic, with measured G_s of 2.64 - 2.67, CBR of 14.6% and shear-box φ of 40˚ - 42˚, and are chemically non-aggressive (Cl^- and SO_3 0.001%) (Paul Kimani & Company, 2018).

The Kizingo VES (**Figure 6**) resolved resistive coral (399 - 642 Ω·m) to 16 - 20 m at VES1 and VES3, underlain by conductive layers of 77 - 82 Ω·m, whereas VES2

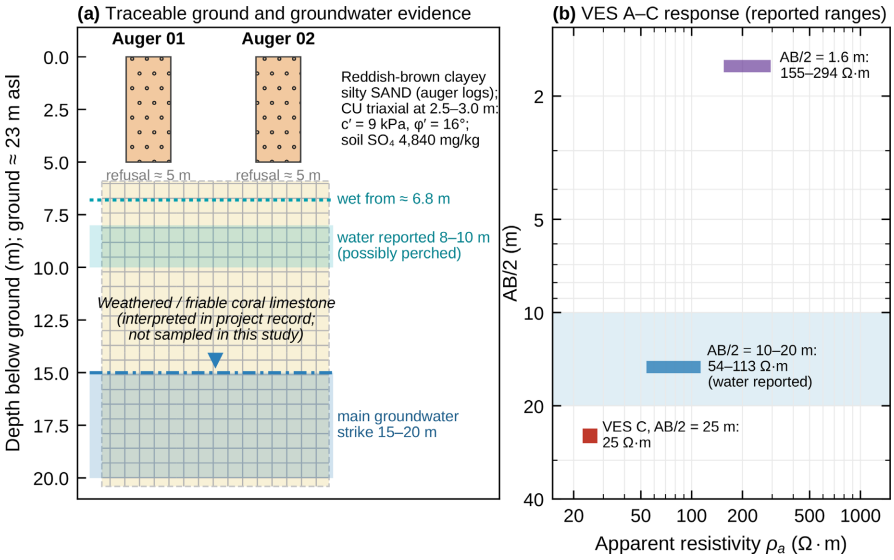


Figure 4. Old Town (Baharini) ground model based on traceable evidence only: (a) auger logs, laboratory data and recorded groundwater observations (ground ≈ 23 m asl); (b) reported VES response ranges (data: ARIDS, 2022).

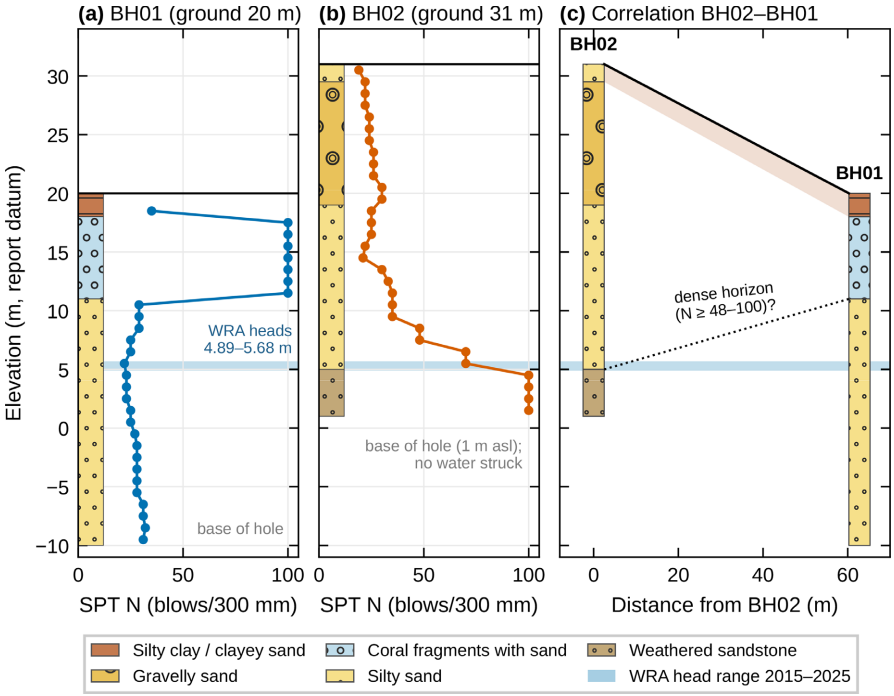


Figure 5. SPT logs of boreholes BH01 and BH02 at Pearl Towers, Tudor, and 2D correlation between them (data: Paul Kimani & Company, 2018).

showed conductive material (58 - 63 Ω·m) from about 4 m. The longitudinal conductance at VES2 (S = 0.30 S) was three to four times that at VES1 (0.11 S) and VES3 (0.07 S). At Old Town, the three VES declined from 155 - 294 Ω·m at AB/2 = 1.6 m to 54 - 113 Ω·m at AB/2 = 10 - 20 m, the depth range in which the project record reports wet ground from 6.8 m, water at 8 - 10 m and a main water strike at about 15 - 20 m (**Figure 4(b)**). The two-dimensional lithological model at Ki-

zingo (Figure 7) shows a thin granular cover over coral that is resistive from 1.25 - 2 m at VES1 and VES3 but conductive from about 4 m at VES2. At Exotica Heights in Nyali, CPT refusal occurred at 1.25 - 1.75 m in the north, whereas cone resistances of 19.6 - 24.5 MPa were reached only at 4 - 5 m in the south, and the VES indicated a deeper conductive horizon at 10 - 14 m.

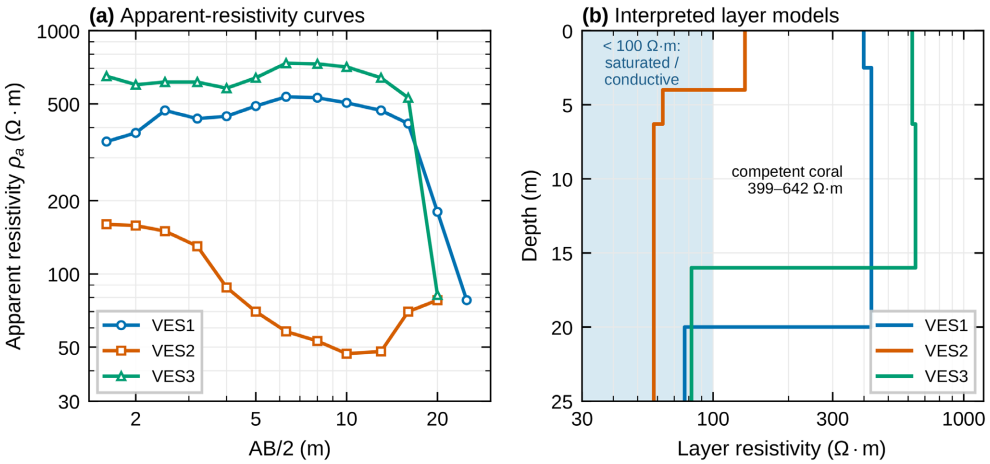


Figure 6. Kizingo VES: (a) apparent-resistivity curves; (b) interpreted layer models (shaded band: <100 Ω·m, saturated or conductive).

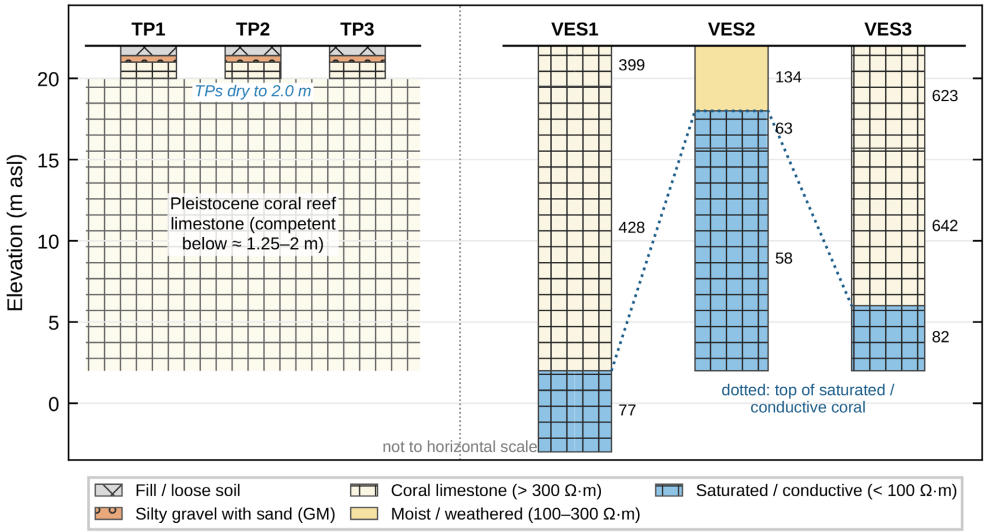


Figure 7. Two-dimensional lithological model of the Kizingo site from trial pits and VES.

Low resistivity can result from saturation, from clay content or from saline pore water, and resistivity alone cannot separate the three. The available evidence constrains, but does not eliminate, the alternatives. At Kizingo, the overburden sampled in the pits is clay-poor (20.5% - 24.4% fines; non-plastic to PI = 3.9%), which argues against a clay-dominated response in the upper metres. With Equation (2), the conductive layers imply pore-water conductivities of 760 - 1920 μS/cm for n = 0.30 - 0.40, i.e., fresh to slightly brackish water rather than seawater (about 50,000 μS/cm), so high salinity is unlikely at Kizingo. These estimates assume a clean formation (a

= 1, m = 2); however, clay-filled weathered coral below the depth of the pits cannot be excluded. The depths to the saturated zone obtained from VES and ERT (Kizingo VES2 ≈ 4 m; Exotica Heights 10 - 14 m; Nyali apartment block 3 - 10 m; Pine Breeze 3 - 5 m) have not been verified by piezometers and are therefore reported as provisional (Table 3). Similarly, the water reported at 6.8 - 10 m at Old Town lies above the main strike at 15 - 20 m, but no low-permeability layer, separate piezometric level or other evidence of hydraulic separation has been documented. It is therefore described as an upper saturated zone that may be perched, not as proven perched groundwater.

Table 3. Depth to groundwater or saturated zone at the investigated sites.

Site	Ground (m asl)	Evidence	Depth to Groundwater/Saturated Zone
Kizingo Trial Pits	22	Measured	Not encountered to 2.0 m
Kizingo VES1/VES3; VES2	≈22	Inferred (VES); provisional	16 - 20 m; ≈4 m
Old Town (Baharini)	23	Recorded in project report; consistent with VES	Wet 6.8 m; upper zone (possibly perched) 8 - 10 m; main 15 - 20 m
Nyali, Exotica Heights	coastal plain	Inferred (VES); provisional	10 - 14 m
Nyali, Apartment Block	coastal plain	Inferred (ERT/MASW); provisional	≈3 - 10 m
Nyali, Pine Breeze	coastal plain	Inferred (ERT); provisional	Saline/saturated conduits from 3 - 5 m
Tudor Creek Margin	low	Measured (WRA heads)	Head 4.89 - 5.68 m asl (shallow, tidal)
Tudor, Pearl Towers	20 - 31	During drilling (no standpipe)	Not struck to 30 m; heads imply ≈ 14 - 26 m
Dongo Kundu SEZ	1.3 - 5.3	Measured	At or near surface

Sources: see Table 1. Geophysically inferred depths are provisional until verified by piezometers; "possibly perched" indicates that hydraulic separation from the main water table has not been demonstrated.

The groundwater evidence is summarised in Table 3 and Figure 8, and integrated in the conceptual section of Figure 9. Beneath the raised coral platform, the main water table lies about 15 - 20 m deep, with an upper saturated zone (possibly perched) from 6.8 m at Old Town and a provisional saturated pocket from about 4 m at Kizingo VES2. Beneath the distressed apartment block in Nyali, the consultant's ERT and MASW interpretation placed the water table at about 3 - 10 m (provisional). On the Tudor Creek margin, WRA heads of 4.89 - 5.68 m asl place the water table within a few metres of the ground and in tidal connection with the creek. Where the ground rises to 20 - 31 m at Pearl Towers, 46 m from a WRA borehole, the same heads lie 14 - 26 m deep; no water was recorded to 30 m during drilling, although readings taken only at shift changes in advancing holes are not stabilised levels. At Dongo Kundu, the onshore ground lies 1.3 - 5.3 m above datum over 30 - 35 m of very soft marine clay (Southern Engineering Company (SECO), 2021).

The lithological correlation panel (Figure 10) contrasts the granular foundation zone of the raised platform with the plastic shale-derived silts of the Mikindani plateau and the 30 - 35 m of very soft marine clay beneath the Dongo Kundu lagoon

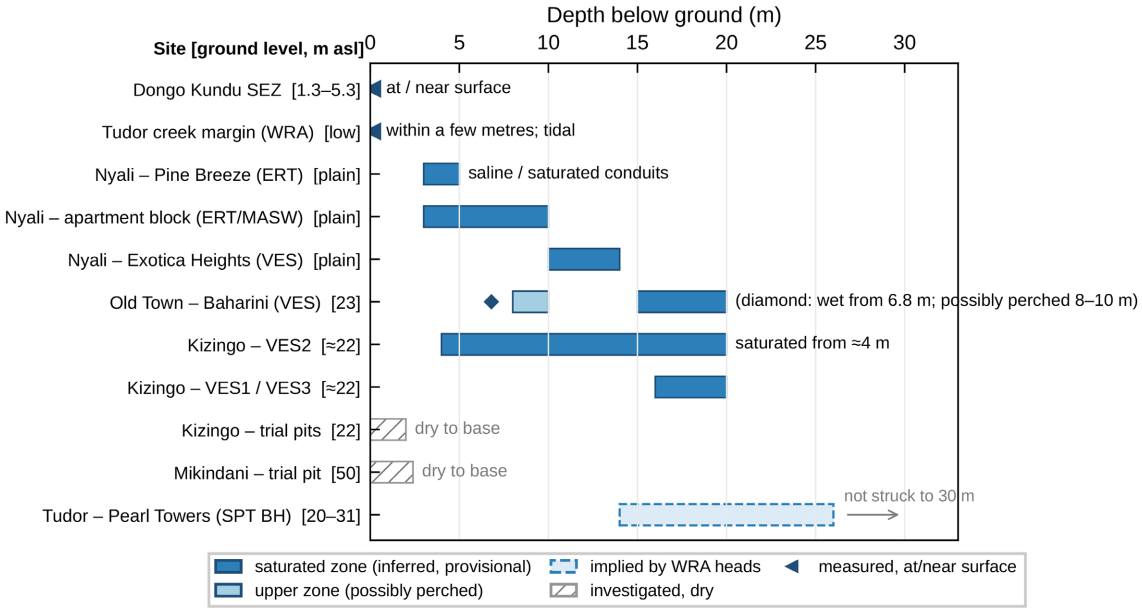


Figure 8. Depth to groundwater or saturated zone at the investigated sites; geophysically inferred depths are provisional.

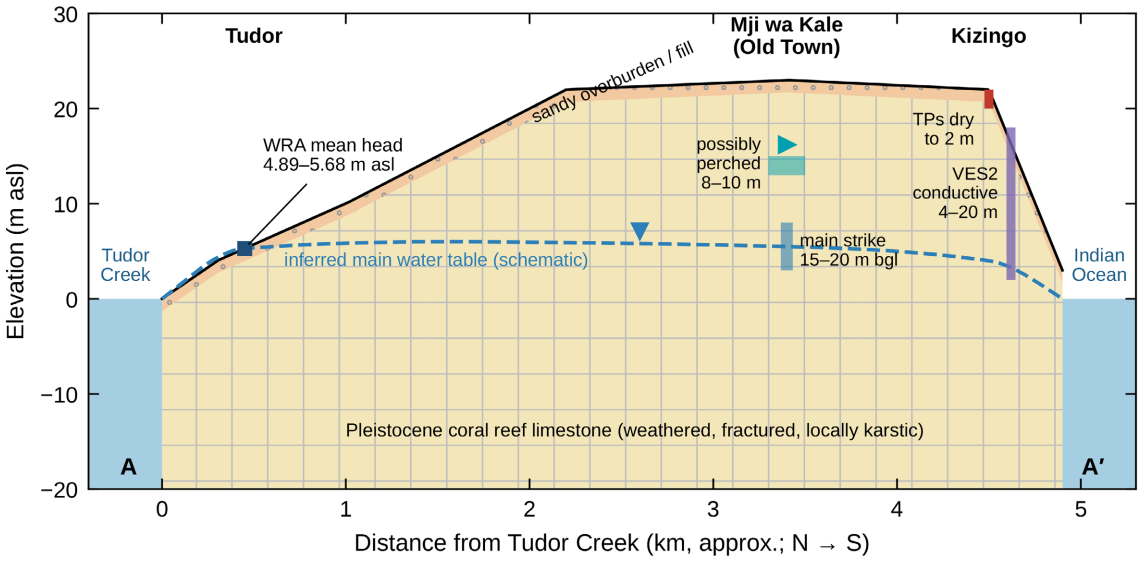


Figure 9. Conceptual A-A' engineering-hydrogeological section across Mombasa Island (vertical exaggeration ≈ 50×); the dashed line is the inferred main water table (schematic).

margin, where competent bearing strata occur only at 33 - 38 m below the sea floor (SECO, 2021).

4.2. Properties of Foundation Materials

The Kizingo overburden is a silty gravel with sand (GM; A-1-b/A-2-6) with 20.5% - 24.4% fines, LL = 25% - 26% and negligible plasticity (Table 4). Its maximum dry density is 1702 - 1772 kg/m^3 at 12.9% - 15.9% optimum moisture, and the re-moulded shear parameters are c' = 5 - 10 kPa and φ' = 21˚ - 25˚. From Equation (3), the void ratio is 0.52 - 0.59 and the degree of saturation of the specimens compacted

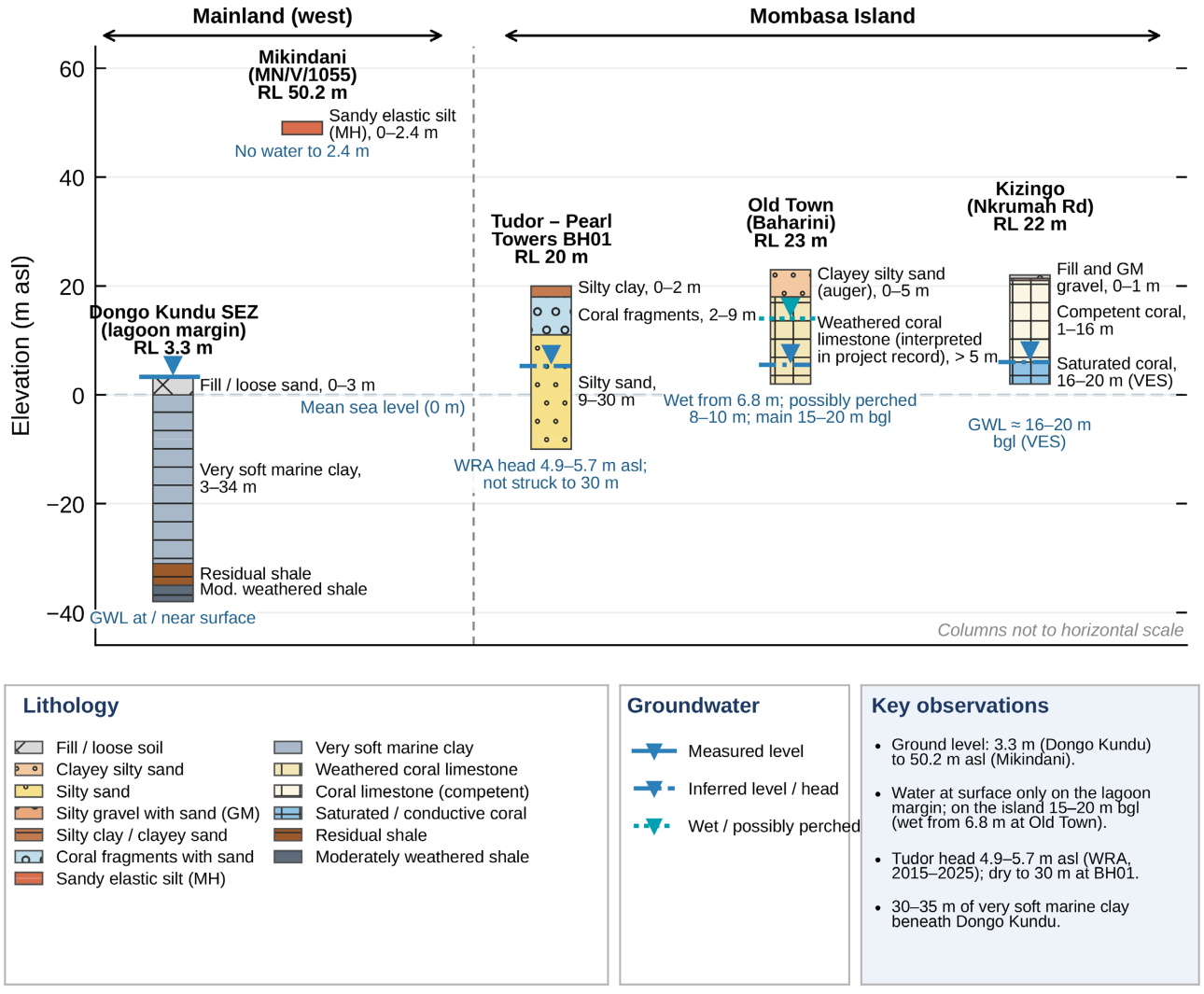


Figure 10. Lithological correlation panel of the investigated sites hung on elevation (m asl), with measured, inferred and possibly perched groundwater levels.

Table 4. Index, compaction, strength and derived phase properties of the Kizingo overburden (0.6 - 1.0 m).

Pit	Gravel/Sand/Fines (%)	LL/PI (%)	MDD (kg/m³)/ OMC (%)	c' (kPa)/φ' (°)	e	S_r at OMC	γ/γ' (kN/m³)	UCS of Coral (MPa)
TP1	41.0/38.5/20.5	25.2/NP	1772/12.9	8/23	0.52	0.67	19.63/10.95	11.27
TP2	47.9/28.3/23.8	25.7/3.9	1702/15.9	10/21	0.59	0.73	19.36/10.51	10.61
TP3	32.7/42.9/24.4	26.1/NP	1750/14.7	5/25	0.54	0.73	19.69/10.81	12.27

Source: laboratory data from CMTC (2025); e, S_r and γ' derived with $G_s = 2.70$; S_r refers to specimens compacted at OMC, not to *in-situ* conditions.

at optimum moisture is 0.67 - 0.73. These values describe laboratory-compacted specimens, not the ground: no *in-situ* moisture content, density or suction was measured, so the field degree of saturation and any suction-derived part of the measured cohesion are not quantified. The submerged unit weight (10.5 - 11.0 kN/m³) is 44% - 46% lower than the moist unit weight (19.4 - 19.7 kN/m³). The coral gave

$I_{s(50)}$ = 0.51 - 0.59 MPa and UCS = 10.6 - 12.3 MPa (weak), with allowable pressures of 400 - 463 kPa in the dry state. At Mikindani, the shale-derived sandy elastic silt (MH; LL 52%, PI 17%) had c' = 14 kPa and φ' = 16˚. DCP tests gave CBR = 10.7% at Kizingo (DN = 19.2 mm/blow) and 7.0% at Mikindani (DN = 28 mm/blow).

The grading curves (Figure 11) are broad and gap-graded, typical of weathered coral debris mixed with sand, and the compaction curves (Figure 12) lie dry of the zero-air-voids line at optimum moisture. This shows only that the compacted specimens were unsaturated; it does not establish the *in-situ* saturation or quantify suction. The effect of suction loss is therefore examined in Section 4.4 as an assumed sensitivity scenario, not as a measured property.

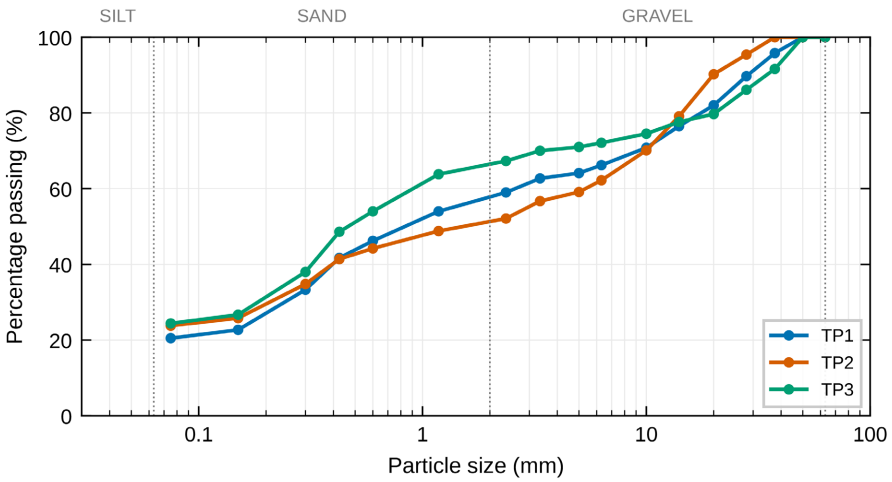


Figure 11. Particle-size distribution of the Kizingo overburden (0.6 - 1.0 m).

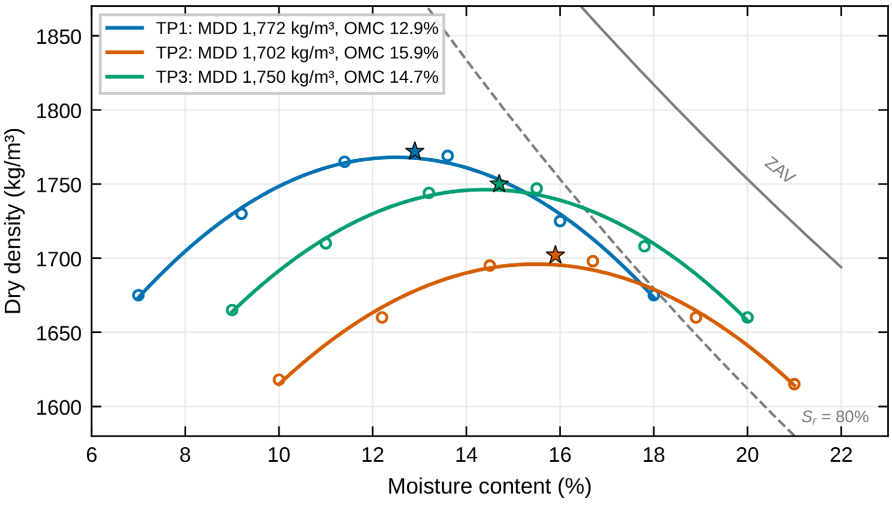


Figure 12. Compaction curves of the Kizingo overburden with zero-air-voids and 80% saturation lines (G_s = 2.70); stars mark the laboratory MDD and OMC.

4.3. Groundwater Aggressiveness

Tudor groundwater (n = 30) contained 62.5 - 2261.3 mg/L sulphate (mean 1015.3 mg/L), 1136 - 15,181 mg/L chloride (mean 5311.5 mg/L) and 10 - 1129 mg/L mag-

nesium, with pH 6.84 - 8.16 (Kithome et al., 2026a). The median, mean, and upper-quartile sulphate values fall in BS EN 206 class XA2 and BRE DS-2/DS-3, and the maximum in XA2/DS-3 (**Table 5**; **Figure 13**). The maximum chloride is about 80% of that of seawater. The chloride exposure class depends on the chloride source and on whether the concrete is permanently immersed or alternately wetted and dried. BS EN 206 assigns chloride from seawater to the XS classes (XS1 airborne salt; XS2 permanently submerged; XS3 tidal, splash and spray zones) and chloride from other sources, such as de-icing salts, industrial brines or effluent, to the XD classes (XD1 moderate humidity; XD2 wet, rarely dry; XD3 cyclic wet and dry). The Tudor chloride is of marine origin: it increases towards the creek, the Cl^-/HCO_3^- ratio rises from 9.1 inland to 64.7 near the coast, and the estimated seawater fraction reaches 48.5% in the coastal zone (Kithome et al., 2026a). The XS classes therefore apply near the creek: XS2 to foundations permanently below the water table and XS3 to concrete in the zone of tidal and seasonal water-table fluctuation, where wetting and drying concentrate chloride. Inland, where the seawater fraction falls to 3.7%, and part of the chloride may come from on-site sanitation, the source is not established; there the more onerous of the XS and XD classes for the same moisture condition (XS2/XD2 if submerged, XS3/XD3 if in the fluctuation zone) is

Table 5. Classification of Tudor groundwater sulphate (n = 30).

Statistic	SO_4^{2-} (mg/L)	BS EN 206	BRE SD1
Minimum	62.5	<XA1	DS-1
Lower Quartile	250.6	XA1	DS-1
Median	790.6	XA2	DS-2
Mean	1,015.3	XA2	DS-2
Upper Quartile	1,469.9	XA2	DS-2/DS-3
Maximum	2,261.3	XA2	DS-3

Source: Computed from Kithome et al. (2026a).

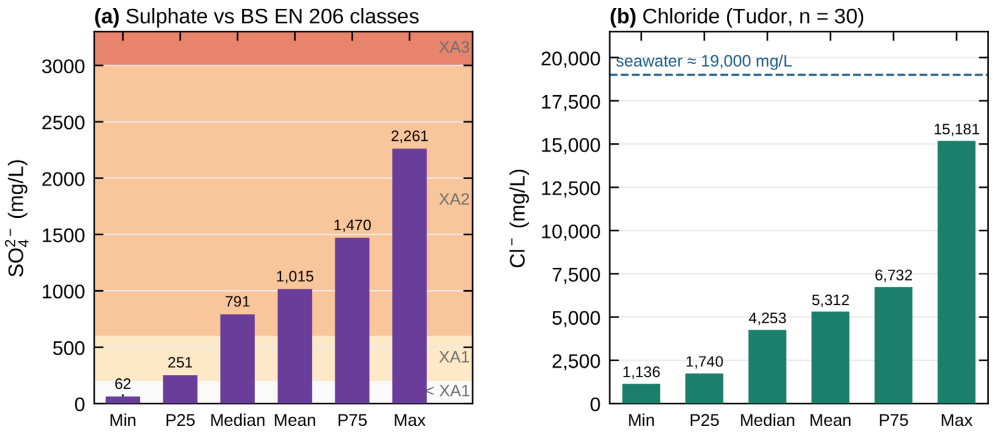


Figure 13. Sulphate and chloride in Tudor groundwater compared with exposure limits.

recommended until the source is confirmed. Old Town soils contained 0.4034% SO_3 (4,840 mg/kg SO_4; XA2) and 104 mg/kg chloride. The Ghyben-Herzberg relation ($z \approx 40h$) indicates that the head decline from 5.68 to 4.89 m asl corresponds to a potential rise of the equilibrium freshwater-saltwater interface from about 227 m to 196 m below sea level, i.e., about 32 m in ten years; because this relation assumes a sharp, steady interface, the value is an equilibrium indicator rather than a measured movement, but it is consistent with the observed salinisation near the creek.

4.4. Effect of Groundwater Rise on Bearing Capacity

At Kizingo, the logged soil cover (fill and silty gravel) ends at about 1.0 m, which is also the footing depth adopted by the laboratory, so a footing at $D_f = 1.0$ m bears on, or very close to, the soil-coral interface. Equations (4) - (7) assume a homogeneous soil extending at least to $D_f + B$ below the base, which is not the case here. The soil-bearing results below are therefore soil-only sensitivity cases: they show how strongly the water table controls the capacity of the granular overburden, which is relevant where the cover is thicker, where footings or ground slabs are founded within the fill and gravel, or where the coral surface is irregular, but they are not design values for footings bearing on the coral. For footings on the coral, the rock-bearing analysis and its softening sensitivity apply. The computed dry allowable pressures (146.4 - 225.5 kPa for $B = 1$ - 4 m and $D_f = 1$ m) agree with the laboratory's values (145 - 224 kPa) to within 1.1%, validating the input parameters. For a 2.0 m footing in TP1 material ($N_c = 21.75$, $N_q = 10.23$, $N_\gamma = 6.00$), the dry, intermediate and flooded cases give:

$$q_{u,dry} = 1.3(8)(21.75) + 19.63(10.23) + 0.4(19.63)(2.0)(6.00) = 521.2 \text{ kPa}; \quad q_a = 173.7 \text{ kPa} \tag{9}$$

$$q_u(D_w = 2.0m) = 226.2 + 200.8 + 0.4(15.29)(2.0)(6.00) = 500.4 \text{ kPa}; \quad q_a = 166.8 \text{ kPa} \tag{10}$$

$$q_u(D_w = 0) = 226.2 + 10.95(10.23) + 0.4(10.95)(2.0)(6.00) = 390.7 \text{ kPa}; \quad q_a = 130.2 \text{ kPa} \tag{11}$$

i.e., a 25.0% reduction when the water table reaches the ground surface. Figure 14 and Figure 15 show that the bearing capacity is unaffected while $D_w > D_f + B$, decreases linearly through the zone of influence, and decreases most steeply above the footing base. The reductions for a water table at the surface are 20% - 34%, increasing with footing width and friction angle (Table 6; Figure 16); the general bearing-capacity equation gives 24% - 33%.

In the assumed scenario in which all of the measured cohesion is suction-derived and is lost on wetting, q_a falls to 41 - 70 kPa for a 2 m footing, 62% - 74% below the dry value; this is an upper-bound sensitivity case, because the *in-situ* suction and its contribution to c' were not measured. In the assumed softening scenario for the coral ($K_s = 0.6$ - 0.9, taken from published values for porous sedimentary rocks because no saturated strength tests were made), the allowable rock pressure

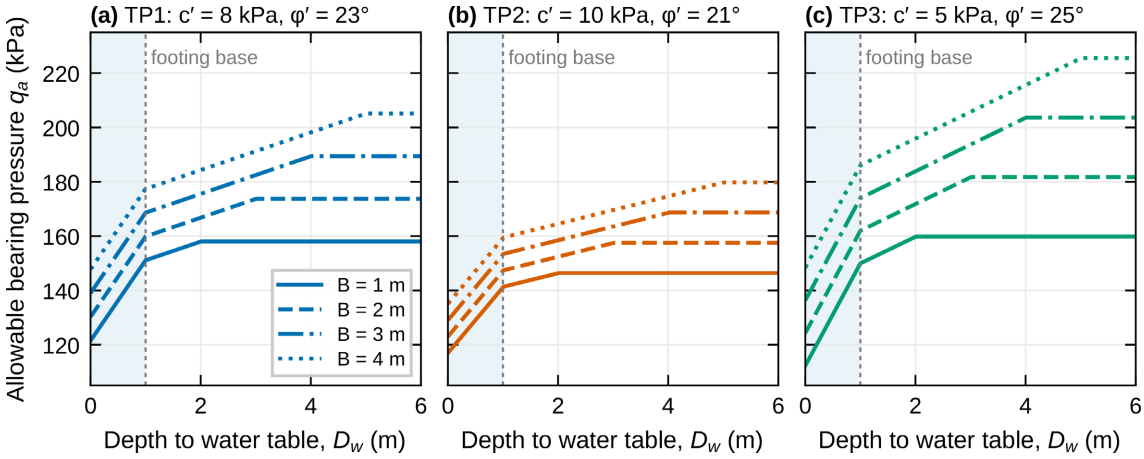


Figure 14. Allowable bearing pressure versus water-table depth, Kizingo overburden (soil-only sensitivity cases; D_f = 1 m; FS = 3).

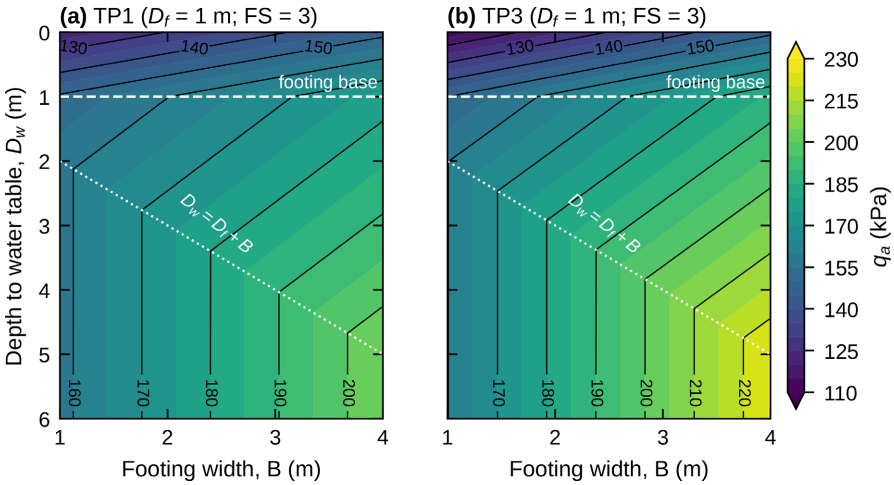


Figure 15. Design charts of allowable bearing pressure (kPa) as a function of footing width and water-table depth, Kizingo TP1 and TP3 (soil-only sensitivity cases). Contours every 10 kPa; the dotted line $D_w = D_f + B$ marks the depth below which the water table no longer affects q_a.

Table 6. Allowable bearing pressure (kPa) for dry and fully saturated conditions, Kizingo overburden, soil-only sensitivity cases (D_f = 1.0 m, FS = 3).

Pit	B (m)	Dry	$D_w = D_f + B/2$	$D_w = 0$	Reduction (%)
TP1	1/2/4	158.0/173.7/205.2	154.6/166.8/191.3	121.5/130.2/147.7	23.1/25.0/28.0
TP2	1/2/4	146.4/157.5/179.8	143.9/152.4/169.6	117.0/123.0/135.1	20.1/21.9/24.8
TP3	1/2/4	159.8/181.7/225.5	154.9/171.8/205.8	112.3/124.3/148.4	29.7/31.6/34.2

Source: Computed in this study.

falls from 400 - 463 kPa to 240 - 416 kPa (Figure 17).

For the Mikindani silt (Figure 18), the reduction on flooding is 18% - 21%, rising to about 50% if the cohesion is halved on wetting.

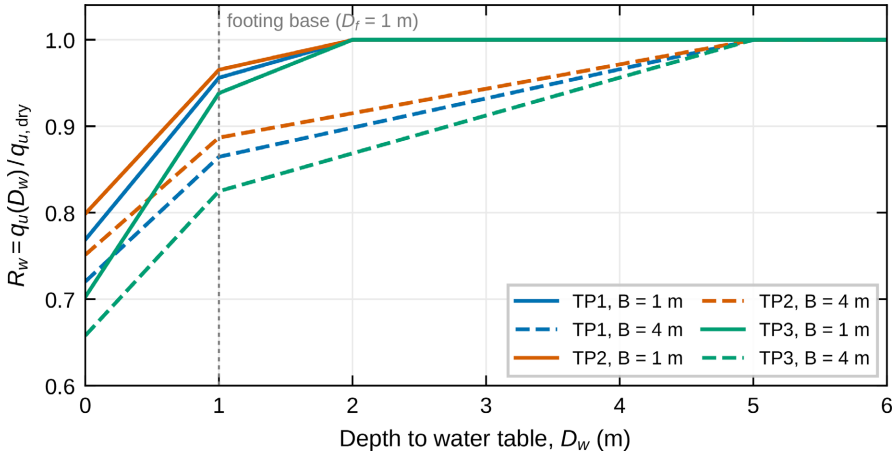


Figure 16. Reduction ratio R_w of ultimate bearing capacity versus water-table depth.

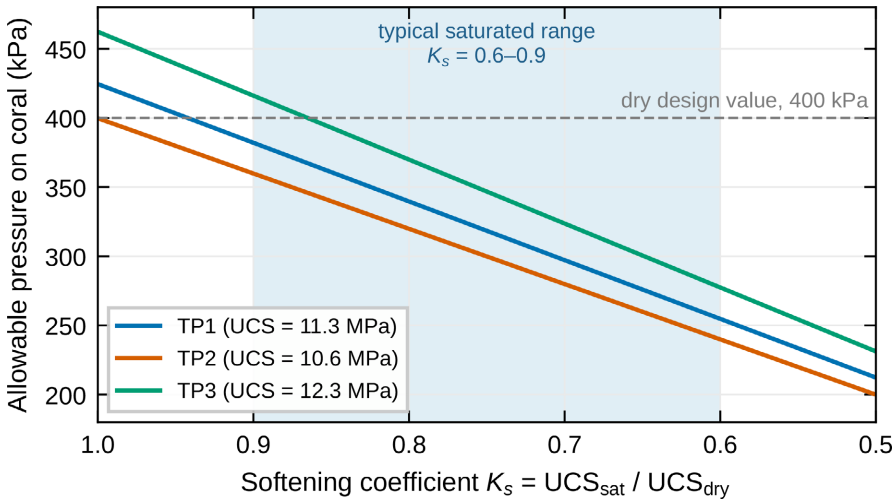


Figure 17. Effect of assumed saturation softening (K_s = 0.6 - 1.0) on the allowable pressure of the Kizingo coral rock.

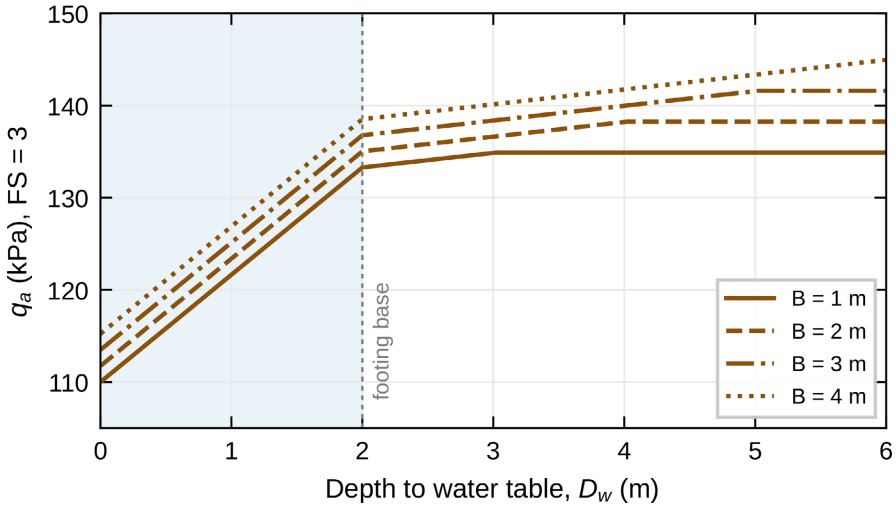


Figure 18. Allowable bearing pressure versus water-table depth for the Mikindani sandy elastic silt (D_f = 2 m).

4.5. Effect on Settlement, Effective Stress, and Uplift

Settlement was evaluated only where measured SPT data exist, at Pearl Towers on the rising ground at Tudor; no settlement analysis is made for Old Town, where no measured penetration data are available. The measured SPT give settlement-controlled allowable pressures (Equation (8)) of 356 - 437 kPa at BH02 and 733 - 893 kPa at BH01 for 2 - 4 m pads at D_f = 1.5 m in dry conditions, which fall to 178 - 218 kPa and 366 - 447 kPa when the ground is flooded (C_w = 0.5) (Table 7). The Burland-Burbidge settlement under a net pressure of 100 kPa doubles, from 3.7 - 5.7 mm to 7.3 - 11.3 mm at BH02 and from 1.3 - 2.1 mm to 2.7 - 4.1 mm at BH01. The heaviest column (8109 kN) on a 4 m pad imposes 507 kPa, more than the dry settlement-controlled capacity at BH02. For these cohesionless sands (c' = 0; cautious φ' = 38˚), Terzaghi's allowable pressure falls from 852 - 1245 kPa to 466 - 681 kPa, a reduction of 45.3% for every width, larger than for the cohesive Kizingo overburden. At present, the WRA heads lie 14 - 26 m below these sites, i.e., below D_f + B, so the flooded case represents a future rise of the water table or ponded flooding rather than current conditions. The vertical effective stress at 1 m and 3 m depth falls by 44% when the water table rises to the surface (Figure 19). Uplift on a basement founded at 3 m reaches 14.7 kPa when the water table is at 1.5 m and 29.4 kPa when it reaches the surface, requiring the equivalent of 1.35 m of concrete, tension piles or relief drainage for a factor of safety of 1.1 (Figure 20).

4.6. Field Evidence from Distressed Structures

Three independent investigations provide field evidence that is consistent with the mechanisms quantified above, although they do not isolate groundwater as the sole cause of distress (Table 8). At an occupied apartment block in Nyali (May 2025), cracks appeared in columns and beams; ERT showed resistivities below 40 Ω·m from 2.5 m to about 15 m beneath the failing column, and MASW recorded V_s < 150 m/s to 15 m and <120 m/s where remedial grouting was under way (Figure 21, Figure 22, Pro-Skill Engineers Hub, 2025). The consultant placed the water table

Table 7. Settlement-controlled allowable pressure (Meyerhof, 25 mm) and Burland-Burbidge settlement of square pads at D_f = 1.5 m, Pearl Towers, Tudor (measured SPT).

Borehole/B (m)	N (Refusal Capped at 50)	q_a dry/ Flooded (kPa)	q_a, D_w = D_f (kPa)	Settlement at 100 kPa, Dry/Flooded (mm)
BH01/2	45.0	893/447	638	1.3/2.7
BH01/3	46.2	783/392	522	1.7/3.4
BH01/4	47.0	733/366	466	2.1/4.1
BH02/2	22.0	437/218	312	3.7/7.3
BH02/3	22.5	381/191	254	4.7/9.4
BH02/4	22.8	356/178	226	5.7/11.3

Source: Computed in this study from the SPT data of Paul Kimani & Company (2018). The WRA heads currently lie below D_f + B at these sites (C_w = 1).

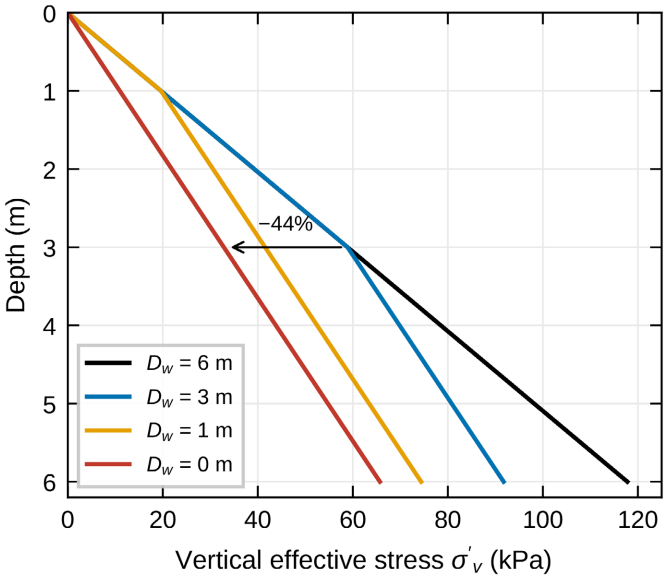


Figure 19. Vertical effective-stress profiles at Kizingo for water-table depths of 6, 3, 1, and 0 m.

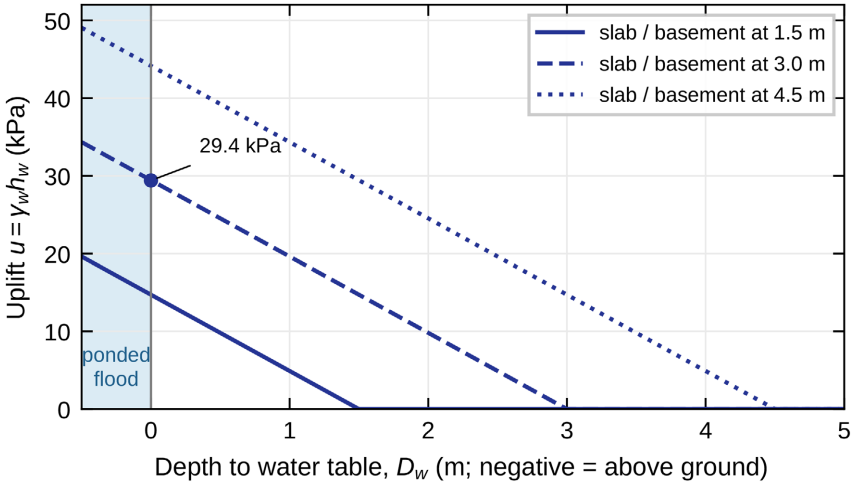


Figure 20. Hydrostatic uplift pressure on slabs and basements versus water-table or flood level.

Table 8. Documented cases of distress associated with saturated or karstic ground in Mombasa.

Case	Distress	Saturated Zone	Ground Weakness
Apartment Block, Nyali (2025)	Cracked columns and beams; grouting	≈3 - 10 m; $\rho < 40$ Ω·m from 2.5 m	$V_s < 120$ - 150 m/s; $N \approx 2$ - 4
Pine Breeze Resort, Nyali (2025)	Cracks 1 - 10 mm after adjacent 3 m excavation	Saline/saturated conduits from 3 - 5 m	Cavities > 1000 Ω·m; $V_s < 200$ m/s at 4 - 12.5 m
Airport Runway Ends (2024)	Depressions, suspected sinkholes	$\rho < 10$ - 20 Ω·m	Cavities within 8 - 10 m
11-Storey Building, Mombasa Island (2025)	Basement caved in; tilting	Weeks of heavy rain	Failed columns; compromised foundation

Sources: Pro-Skill Engineers Hub (2024; 2025); Pine Breeze Report (2025); Oduor (2025); Hussein (2025).

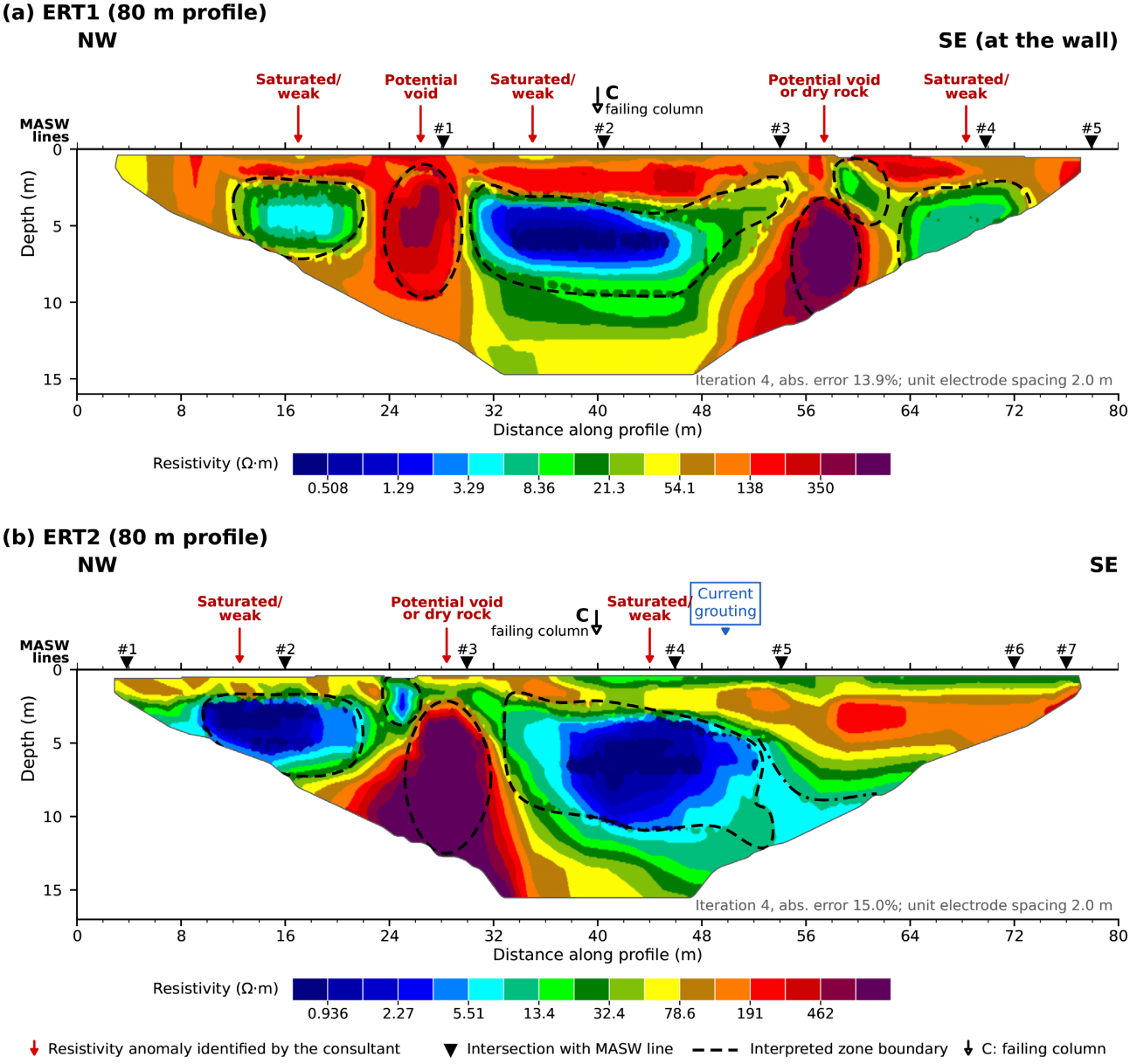


Figure 21. Interpreted ERT1 (top) and ERT2 (bottom) resistivity sections at the distressed apartment block, Nyali, as reported by the consultant (Pro-Skill Engineers Hub, 2025). Black arrows mark the intersections with the MASW lines (MASW#1 - #7); "C" marks the failing column; red arrows mark the positions of the resistivity anomalies highlighted by the consultant; the boxed label marks the remedial grouting underway at the time of the survey.

at about 3 - 10 m (provisional) and interpreted the weak zones as saturated, soft-filled karstic depressions or poorly compacted fill 2 - 10 m deep. Converting the velocities with Imai and Tonouchi (1982):

$$N = \left(V_s/97\right)^{1/0.314} = \left(150/97\right)^{3.185} = 4.0;\ G_0 = \rho V_s^2 = 1.9\times 150^2 = 42.8\ MPa \qquad (12)$$

so the ground beneath the failing column corresponds to $N \approx 2$ - 4 and $G_0 \approx 27$ - 43 MPa, i.e., very loose or very soft material. These correlation-based values are indicative and were not used to compute bearing pressures. At Pine Breeze Holiday Resort in Nyali (August 2025; **Figure 23**), cracks of 1 - 10 mm developed in

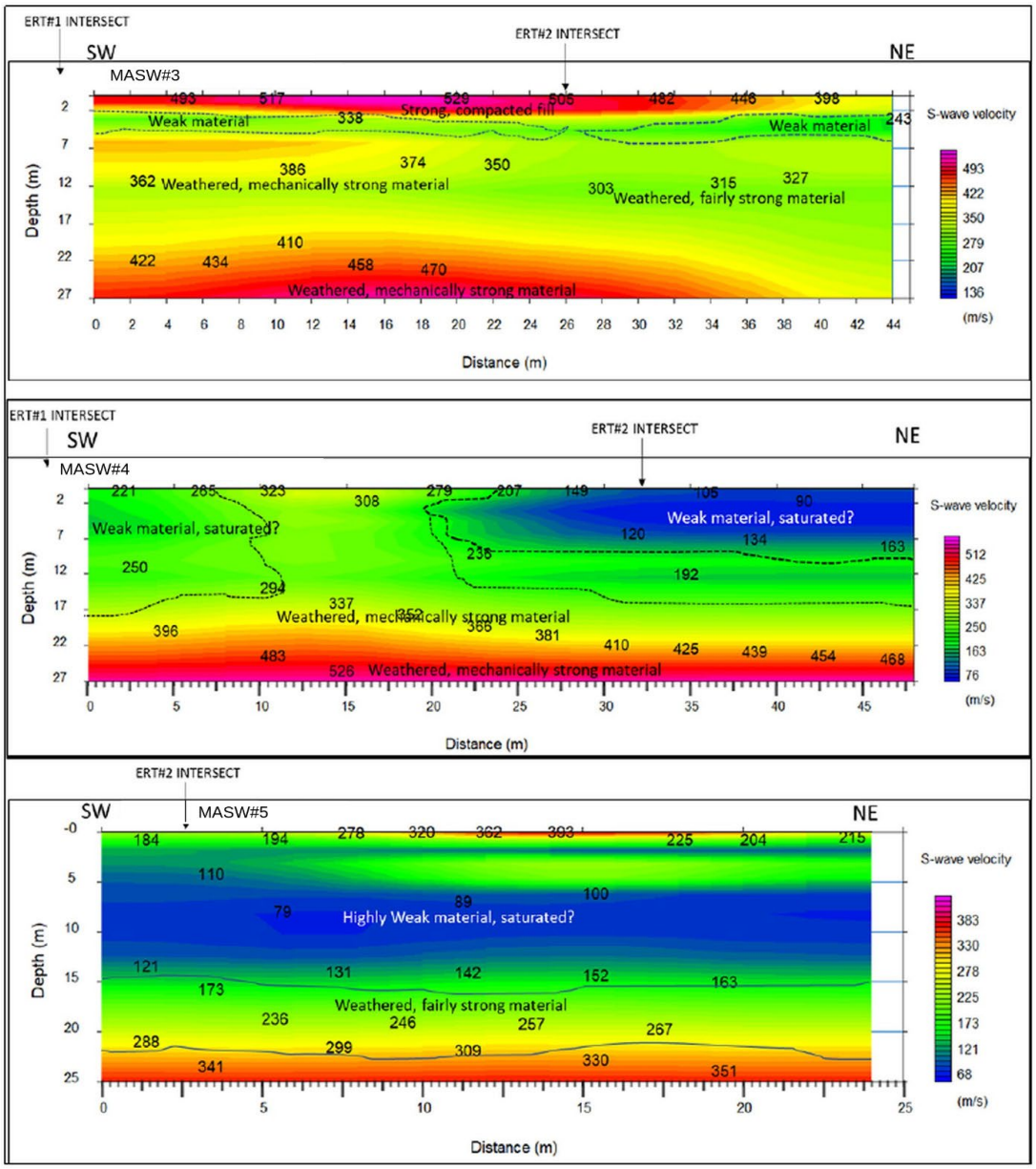


Figure 22. Interpreted MASW shear-wave velocity sections MASW#3 (top), MASW#4 (middle) and MASW#5 (bottom) adjacent to the failing column, Nyali, with the ERT1 and ERT2 intersections marked; velocities in m/s (Pro-Skill Engineers Hub, 2025).

columns, walls, floors and pavements after a 3 m excavation next door; ERT showed cavities (>1000 Ω·m) and saline or saturated conduits (<10 Ω·m) from 3 - 5 m, and MASW showed velocity depressions (V_s < 200 m/s) at 4 - 12.5 m within otherwise stiff ground (V_{s30} = 510 - 591 m/s). At the runway ends of Moi International Airport (May 2024), ERT imaged near-surface cavities within 8 - 10 m above saturated, low-resistivity (<10 - 20 Ω·m) ground where depressions and suspected sinkholes had formed (Pro-Skill Engineers Hub, 2024). Foundation geometry, loading, workmanship and excavation effects were not investigated at these sites, so the cases show a spatial association between weak, saturated or cavernous ground and distress rather than proof of a single cause.



Figure 23. Pine Breeze Holiday Resort, Nyali (August 2025): (a, c, e) geophysical data acquisition; (b) ground cracking beside the adjacent excavation; (d) wall cracking; (f) the adjacent excavation exposing cavernous coral.

5. Discussion

5.1. Controls on the Depth to Groundwater

The results show that the depth to groundwater beneath Mombasa Island is controlled by elevation and by the karstic structure of the coral limestone. Beneath the raised platform, heads of a few metres above sea level beneath ground at 22 - 23 m produce a deep (about 15 - 20 m) main water table, but provisional upper saturated zones occur from about 4 - 7 m, and they vary over tens of metres, as shown by the contrast between VES2 and VES1/VES3 at Kizingo and by the CPT variability at Exotica Heights. This alternation of competent and incompetent zones is typical of reef limestones (Zhu et al., 2017; Zheng et al., 2020). Even at Tudor, the depth to water ranges from a few metres beside the creek to 14 m or more beneath ground, rising to 20 - 31 m, so the creek-margin setting is defined by elevation relative to the groundwater head. On the creek and lagoon margins, the water table is at or near the surface and tidally connected, and is expected to rise approximately with sea level, as shown for other coastal cities (Rotzoll & Fletcher, 2013; Befus et al., 2020; Bosserelle et al., 2022). Shallow trial pits alone cannot detect these conditions; geophysics calibrated by drilling and piezometers is needed to locate and verify them (Loke et al., 2013; Alam et al., 2024).

5.2. Magnitude of the Groundwater Effect

The computed reductions of 20% - 34% in the soil-only cases when the water table

reaches the surface are consistent with the theoretical treatment of Das and Sivakugan (2019) and with the experimental and numerical results of Chen et al. (2022; 2023), who reported bearing-capacity losses of up to 50% for rising water levels and further losses under wetting-drying cycles. A footing designed in the overburden at the dry allowable pressure of 173.7 kPa would have an effective factor of safety of only 2.25 when the ground is saturated, and less than 1.0 in the assumed scenario of complete suction loss. In the dense Tudor sands, the settlement-controlling pressure halves and the computed settlement doubles when the ground floods, and uplift of about 10 kPa per metre of submergence acts on slabs and basements. The Nyali cases are consistent with these mechanisms: cracked columns overlie saturated, very loose ($N \approx 2$ - 4) ground with a water table at about 3 - 10 m, and excavation beside cavernous coral with shallow saline conduits was followed by cracking of adjacent buildings.

5.3. Durability Implications

The Tudor groundwater is aggressive to concrete (XA2; DS-2 to DS-3) and strongly chloride-bearing, and its aggressiveness is linked to seawater intrusion driven by abstraction and the decline of freshwater heads (Werner et al., 2013; Oiro & Comte, 2019; Kithome et al., 2026a). Combined sulphate and chloride exposure accelerates concrete deterioration under wetting and drying (Sun et al., 2022; Zhang et al., 2024), and rising saline groundwater has been identified as a "hidden threat" to buried infrastructure (Habel et al., 2024). A calibrated SEAWAT model of the Tudor aquifer (head RMSE = 0.38 m, $R^2 = 0.89$; chloride RMSE = 892 mg/L, $R^2 = 0.94$) placed the 5,000 mg/L and 1,000 mg/L isochlors about 2.5 km and 5.5 km inland in 2025 (Kithome et al., 2026b). Foundations near the creeks should therefore use sulphate-resisting blended binders (CEM III/B, IV/B or II/B-V), a water/cement ratio not exceeding 0.45, a binder content of at least 360 - 380 kg/m^3 and a nominal cover of at least 60 mm, with waterproofing where the water table fluctuates (**Table 9**; BRE, 2005; BSI, 2023).

Table 9. Indicative concrete durability requirements for foundations in Mombasa.

Setting	Exposure	Binder	Max. w/c	Min. Binder (kg/m^3)	Cover (mm)
Creek margin (Tudor, Dongo Kundu)	XA2 (DS-2/DS-3); XS2 (submerged); XS3 (water-table fluctuation zone)	CEM III/B, IV/B, II/B-V	0.45	360 - 380	≥ 60
Raised platform, below water table	XA2 (soil); XS2, or XS2/XD2 where chloride source is unconfirmed	CEM III/B or II/B-V	0.45 - 0.50	340 - 360	≥ 50
Raised platform, above water table	XA1-XA2 (soil); XS1 (marine atmosphere)	CEM II or III	0.50	320 - 340	≥ 50

Indicative values from BS EN 206, BS 8500-1 and BRE SD1; final specification to be selected from the code tables.

5.4. Implications for Design and Planning

Three settings emerge (**Table 10**): (A) creek and lagoon margins with a permanently shallow, tidal and aggressive water table, where piled or raft foundations, anti-flota-

tion design and durable concrete are required; (B) some parts of the platform and the Nyali coastal plain with upper saturated zones and karstic weak zones, where footings should bypass loose soils to competent coral, cavities should be probed and grouted, and excavations beside existing buildings should be supported and monitored; and (C) the elevated platform, where competent coral lies near the surface and the main risk arises from local pockets and transient saturation. In all settings, the design groundwater level should be taken as the highest credible level, including possibly perched water and flooding, and site investigations should include geophysics calibrated by drilling, piezometers, *in-situ* suction or moisture measurements and saturated strength tests.

Table 10. Groundwater-related hazard zonation for foundations on Mombasa Island and adjoining areas.

Zone	Examples	Groundwater	Effect of Saturation on q_a	Exposure	Foundation Approach
A: Creek and lagoon margins	Tudor Creek margin; Dongo Kundu	At/near surface; tidal; rising with sea level	−20% to −45%; permanent uplift	High (XA2; XS2 submerged, XS3 fluctuation zone)	Piles or raft on improved ground; anti-flotation; durable concrete
B: Platform with upper saturated zones; Nyali coastal plain	Old Town; Nyali	Upper zone (possibly perched) 4 - 10 m; main 15 - 20 m	−20% to −34% (soil-only); up to −74% if suction is lost (assumed)	Moderate (soil XA2)	Found on competent coral; probe and grout cavities; drainage
C: Elevated coral platform	Kizingo (VES1/VES3); Tudor rising ground (Pearl Towers)	≥ 14 - 20 m; local pockets	−20% to −34% (soil-only); −45% (dense sand); −10% to −40% (rock, assumed softening)	Low-moderate	Embed ≥ 250 mm in probed competent coral; positive drainage

Source: Synthesised from this study. The limitations of the study, namely the shallow direct exploration, the provisional geophysical water depths, the assumed suction-loss and softening scenarios, the remoulded shear specimens and the assumed specific gravity, mean that the computed values are design-level estimates that should be confirmed by site-specific drilling, piezometric monitoring and saturated testing.

6. Conclusion

1) The main water table beneath the raised coral platform of Mombasa Island lies about 15 - 20 m deep, with provisional upper saturated zones from about 4 - 7 m; beneath the Tudor Creek margin, the Dongo Kundu lagoon margin and parts of Nyali, the water table is at or within about 3 - 10 m of the surface, whereas on the rising ground at Tudor (Pearl Towers) the same heads lie 14 - 26 m deep. Geophysically inferred depths remain provisional until verified by piezometers.

2) The foundation soils are silty gravels and sands (c' = 5 - 10 kPa; φ' = 21˚ - 25˚) over weak coral (UCS = 10.6 - 12.3 MPa); submergence reduces their effective unit weight by 44% - 46%.

3) Tudor groundwater is aggressive to concrete: its sulphate places it in XA2 (DS-2 to DS-3), and its chloride (up to 15,181 mg/L), which is of marine origin, places submerged foundations in XS2 and concrete in the water-table fluctuation zone in XS3. Old Town soils contain 4840 mg/kg sulphate (XA2).

4) In soil-only sensitivity cases, a rise of the water table to the surface reduces the allowable bearing pressure of the Kizingo overburden by 20% - 34%; it also reduces the bearing capacity of the dense Tudor sands by 45%, halves their settlement-controlled pressure, doubles their computed settlement, and imposes uplift of 9.8 kPa per metre of submergence. Assumed scenarios of suction loss (62% - 74% reduction) and coral softening (10% - 40% reduction) indicate that the margins could be smaller still; these scenarios should be checked by *in-situ* suction measurement and saturated strength testing.

5) Documented distress at two Nyali sites and ground depressions at the airport coincide with saturated, low-stiffness or cavernous ground. Together with the computed effects, this indicates that the groundwater table should be treated as a design variable in Mombasa. Piezometric monitoring, geophysical screening calibrated by drilling, saturated strength testing, durable concrete specification and drainage rehabilitation are recommended.

Author Contributions

Charles Ngala Kithome: Conceptualization, methodology, investigation, field data collection, geotechnical and hydrogeological analysis, geophysical data interpretation, formal analysis, visualization, and writing—original draft preparation. **Edwin W. Dindi:** Supervision, methodological guidance, technical validation, interpretation of results, and writing—review and editing. **Charles Maina Gichaba:** Supervision, methodological review, technical validation, critical evaluation of findings, and writing—review and editing. All authors reviewed and approved the final version of the manuscript.

Acknowledgements

The authors thank the Water Resources Authority (Coast Region), Cransfield Material Testing Centre, ARIDS-Kenya, Southern Engineering Company and Pro-Skill Engineers Hub for access to data, and the Department of Earth and Climate Sciences, University of Nairobi, for academic support.

Conflicts of Interest

The authors declare no conflicts of interest regarding the publication of this paper.

References

Alam, M. J. B., Ahmed, A., & Alam, M. Z. (2024). Application of Electrical Resistivity Tomography in Geotechnical and Geoenvironmental Engineering Aspect. *Geotechnics, 4,* 399-414. https://doi.org/10.3390/geotechnics4020022

American Public Health Association (APHA), American Water Works Association, & Water Environment Federation (2023). *Standard Methods for the Examination of Water and Wastewater* (24th ed.). APHA Press.

Aqua Rural Infrastructure Development Solutions (ARIDS) (2022). *Geophysical and Geoengineering Site Characterization for Foundation Integrity Survey Report for Baharini Luxury Apartments Limited, L.R. No. MI/XLVI/123 to 126, Mji wa Kale, Mvita, Mombasa*

County [Unpublished Consultancy Report]. ARIDS-Kenya.

Aqua Rural Infrastructure Development Solutions (ARIDS) (2026). *Integrated Geotechnical and Geophysical Investigation Report: Exotica Heights Apartments, Nyali, Mombasa County (Report ARIDS/EXH/GIR/2026-01, Rev. 00)* [Unpublished Consultancy Report]. ARIDS-Kenya.

Archie, G. E. (1942). The Electrical Resistivity Log as an Aid in Determining Some Reservoir Characteristics. *Transactions of the AIME, 146,* 54-62. https://doi.org/10.2118/942054-g

Befus, K. M., Barnard, P. L., Hoover, D. J., Finzi Hart, J. A., & Voss, C. I. (2020). Increasing Threat of Coastal Groundwater Hazards from Sea-Level Rise in California. *Nature Climate Change, 10,* 946-952. https://doi.org/10.1038/s41558-020-0874-1

Bosserelle, A. L., Morgan, L. K., & Hughes, M. W. (2022). Groundwater Rise and Associated Flooding in Coastal Settlements Due to Sea-Level Rise: A Review of Processes and Methods. *Earth's Future, 10,* e2021EF002580. https://doi.org/10.1029/2021ef002580

Bowles, J. E. (1996). *Foundation Analysis and Design* (5th ed.). McGraw-Hill.

British Standards Institution (BSI) (2021). *Concrete: Specification, Performance, Production and Conformity* (BS EN 206:2013+A2:2021). BSI.

British Standards Institution (BSI) (2023). *Concrete: Complementary British Standard to BS EN 206. Part 1: Method of Specifying and Guidance for the Specifier* (BS 8500-1:2023). BSI.

Building Research Establishment (BRE) (2005). *Concrete in Aggressive Ground* (BRE Special Digest 1, 3rd ed.). BRE Press.

Burland, J. B., & Burbidge, M. C. (1985). Settlement of Foundations on Sand and Gravel. *Proceedings of the Institution of Civil Engineers, 78,* 1325-1381. https://doi.org/10.1680/iicep.1985.1058

Caswell, P. V. (1953). *Geology of the Mombasa-Kwale Area* (Report No. 24). Geological Survey of Kenya.

Chen, W., Liu, Q., & Wang, E. (2022). The Effect of the Water Table on the Bearing Capacity of a Shallow Foundation. *Applied Sciences, 12,* Article 6571. https://doi.org/10.3390/app12136571

Chen, W., Xia, W., Zhang, S., & Wang, E. (2023). Study on the Influence of Groundwater Variation on the Bearing Capacity of Sandy Shallow Foundation. *Applied Sciences, 13,* Article 473. https://doi.org/10.3390/app13010473

Cransfield Material Testing Centre (CMTC) (2025). *Geotechnical Investigation Report for the Proposed Cairo Hotel, Nkrumah Road, Kizingo Area, Mombasa County* [Unpublished Report, September 2025]. CMTC, in Collaboration with ARIDS-Kenya.

Cransfield Material Testing Centre (CMTC) (2026). *Geotechnical Investigation Report for the Proposed Mil Block on Plot No. MN/V/1055, Mombasa County* [Unpublished Report, May 2026]. CMTC.

Das, B. M., & Sivakugan, N. (2019). *Principles of Foundation Engineering* (9th ed.). Cengage Learning.

Goodman, R. E. (1989). *Introduction to Rock Mechanics* (2nd ed.). John Wiley & Sons.

Habel, S., Fletcher, C. H., Anderson, T. R., & Thompson, P. R. (2020). Sea-Level Rise Induced Multi-Mechanism Flooding and Contribution to Urban Infrastructure Failure. *Scientific Reports, 10,* Article No. 3796. https://doi.org/10.1038/s41598-020-60762-4

Habel, S., Fletcher, C. H., Barbee, M. M., & Fornace, K. L. (2024). Hidden Threat: The Influence of Sea-Level Rise on Coastal Groundwater and the Convergence of Impacts on Mu-

nicipal Infrastructure. *Annual Review of Marine Science, 16,* 81-103. https://doi.org/10.1146/annurev-marine-020923-120737

Hawkins, A. B., & McConnell, B. J. (1992). Sensitivity of Sandstone Strength and Deformability to Changes in Moisture Content. *Quarterly Journal of Engineering Geology, 25,* 115-130. https://doi.org/10.1144/gsl.qjeg.1992.025.02.05

Hill, K., Hirschfeld, D., Lindquist, C., Cook, F., & Warner, S. (2023). Rising Coastal Groundwater as a Result of Sea-Level Rise Will Influence Contaminated Coastal Sites and Underground Infrastructure. *Earth's Future, 11,* e2023EF003825. https://doi.org/10.1029/2023ef003825

Hussein, F. (2025). *AAK Attributes Cracks in Mombasa Building Teetering on Collapse to Structural Failures*. The Eastleigh Voice. https://eastleighvoice.co.ke/coast/134110/aak-blames-structural-failures-for-mombasa-building-teetering-on-collapse

Imai, T., & Tonouchi, K. (1982). Correlation of N Value with S-Wave Velocity and Shear Modulus. In A. Verruijt (Ed.), *Penetration Testing* (pp. 67-72). Routledge. https://doi.org/10.1201/9780203743959-11

Kagema, A., & Muzirafuti, A. (2026). Assessment of Coastal Vulnerability to Sea Level Rise: A Case Study of the Kenyan Coastline. *Frontiers in Marine Science, 13,* Article ID: 1812200. https://doi.org/10.3389/fmars.2026.1812200

Kenya National Bureau of Statistics (KNBS) (2019). *2019 Kenya Population and Housing Census: Volume I. Population by County and Sub-County*. KNBS.

Kithome, C. N., Makokha, M., & Murimi, S. (2026a). Quantifying Seawater Intrusion in a Stressed Coastal Aquifer Using Hydrochemical and Statistical Analysis: Evidence from the Tudor Aquifer, Kenya. *Journal of Geoscience and Environment Protection, 14,* 49-63. https://doi.org/10.4236/gep.2026.145005

Kithome, C. N., Makokha, M., & Murimi, S. (2026b). Variable-Density Modelling of Groundwater Abstraction, Sea-Level Change and Managed Recharge in the Tudor Coastal Aquifer, Mombasa, Kenya. *Journal of Geoscience and Environment Protection, 14,* 213-233. https://doi.org/10.4236/gep.2026.149012

Loke, M. H., Chambers, J. E., Rucker, D. F., Kuras, O., & Wilkinson, P. B. (2013). Recent Developments in the Direct-Current Geoelectrical Imaging Method. *Journal of Applied Geophysics, 95,* 135-156. https://doi.org/10.1016/j.jappgeo.2013.02.017

Meyerhof, G. G. (1965). Shallow Foundations. *Journal of the Soil Mechanics and Foundations Division, 91,* 21-31. https://doi.org/10.1061/jsfeaq.0000719

Oduor, F. (2025). *Mombasa Residents Evacuated as Cracks in 11-Storey Building Raise Collapse Fears*. Kenyans.co.ke. https://www.kenyans.co.ke/news/110632-mombasa-residents-evacuated-cracks-11-storey-building-raise-collapse-fears

Oiro, S., & Comte, J. (2019). Drivers, Patterns and Velocity of Saltwater Intrusion in a Stressed Aquifer of the East African Coast: Joint Analysis of Groundwater and Geophysical Data in Southern Kenya. *Journal of African Earth Sciences, 149,* 334-347. https://doi.org/10.1016/j.jafrearsci.2018.08.016

Omanga, A. (2024). *Flood Risk Assessment of Mombasa County, Kenya: Technical Report*. Covenant of Mayors in Sub-Saharan Africa, & County Government of Mombasa. https://comssa.org/download/qbkGc8npDQF7WsexEoMVYjfrgRPH05C1/Mombasa-Flood-Risk-Assessment-Technical-Report.pdf

Paige-Green, P., & Du Plessis, L. (2009). *The Use and Interpretation of the Dynamic Cone Penetrometer (DCP) Test* (Version 2). CSIR Built Environment.

Park, C. B., Miller, R. D., & Xia, J. (1999). Multichannel Analysis of Surface Waves. *Geo-*

physics, 64, 800-808. https://doi.org/10.1190/1.1444590

Paul Kimani & Company Ltd. (2018). *Geotechnical Investigation for the Proposed Pearl Towers Development on Plot No. MI/X/75, Tudor, Mombasa County: Engineering Report* [Unpublished Consultancy Report].

Pine Breeze Report (2025). *Geophysical Investigation Preliminary Report: Pine Breeze Holiday Resort, Nyali, Mombasa County, Kenya.* [Unpublished Consultancy Report, Survey August 2025].

Pro-Skill Engineers Hub (2024). *Geophysical Investigation Report: Electrical Resistivity Tomography at the Runway Terminal Ends, Moi International Airport, Mombasa County, Kenya (Survey date 14 May 2024)* [Unpublished Consultancy Report].

Pro-Skill Engineers Hub (2025). *Geophysical Investigation Report: ERT and MASW Investigation of Structural Distress at an Apartment Block, Nyali, Mombasa County, Kenya* (Survey Date 30 May 2025) [Unpublished Consultancy Report].

Richardson, C. M., Davis, K. L., Ruiz-González, C., Guimond, J. A., Michael, H. A., Paldor, A. et al. (2024). The Impacts of Climate Change on Coastal Groundwater. *Nature Reviews Earth & Environment, 5,* 100-119. https://doi.org/10.1038/s43017-023-00500-2

Rotzoll, K., & Fletcher, C. H. (2013). Assessment of Groundwater Inundation as a Consequence of Sea-Level Rise. *Nature Climate Change, 3,* 477-481. https://doi.org/10.1038/nclimate1725

Southern Engineering Company (SECO) (2021). *Geotechnical Factual Report on the Detailed Design for the Mombasa Special Economic Zone Development Project* [Report Prepared for Nippon Koei Co. Ltd]. SECO.

Sun, D., Cao, Z., Huang, C., Wu, K., De Schutter, G., & Zhang, L. (2022). Degradation of Concrete in Marine Environment under Coupled Chloride and Sulfate Attack: A Numerical and Experimental Study. *Case Studies in Construction Materials, 17,* e01218. https://doi.org/10.1016/j.cscm.2022.e01218

The Star (2023). *Explainer: Why Mombasa Is Experiencing Serious Flooding*. The Star. https://www.the-star.co.ke/counties/central/2023-11-20-explainer-why-mombasa-is-experiencing-serious-flooding

Vásárhelyi, B., & Ván, P. (2006). Influence of Water Content on the Strength of Rock. *Engineering Geology, 84,* 70-74. https://doi.org/10.1016/j.enggeo.2005.11.011

Werner, A. D., Bakker, M., Post, V. E. A., Vandenbohede, A., Lu, C., Ataie-Ashtiani, B. et al. (2013). Seawater Intrusion Processes, Investigation and Management: Recent Advances and Future Challenges. *Advances in Water Resources, 51,* 3-26. https://doi.org/10.1016/j.advwatres.2012.03.004

Zhang, C., Li, J., Yu, M., Lu, Y., & Liu, S. (2024). Mechanism and Performance Control Methods of Sulfate Attack on Concrete: A Review. *Materials, 17,* Article 4836. https://doi.org/10.3390/ma17194836

Zheng, K., Meng, Q., Wang, R., Yu, J., Wu, W., & Yu, K. (2020). Advances in Study of Engineering Geological Characteristics of Coral Reef Limestone. *Marine Geology & Quaternary Geology, 40,* 42-49.

Zhu, C. Q., Liu, H. F., Wang, X., Meng, Q. S., & Wang, R. (2017). Engineering Geotechnical Investigation for Coral Reef Site of the Cross-Sea Bridge between Malé and Airport Island. *Ocean Engineering, 146,* 298-310. https://doi.org/10.1016/j.oceaneng.2017.09.039